ALKOR-Berichte

Studierendenbericht zum Seepraktikum Geophysik 2020 (UHH)

Cruise No. AL545

18.09.-28.09.2020,
Kiel (Germany) – Kiel (Germany)
Seeprak'20-UHH

C. Hübscher, Aster, M.S., Behr, C., Bogner, L., Chung, J.I., Devdariani, A., Dittmers, C., Ehlies, V., Eßbach, V., Häcker, T., Lackner, M., Maaß, R., Preine, J., Rehm, A., Uhl, K.J., Wodke, V.

Chief Scientist: Christian Hübscher
Universität Hamburg

2020

Table of Contents

1 Cruise Summary

(C. Hübscher, T. Häcker, J. Preine)

1.1 Summary in English

The student exercise cruise AL545, in which a total of 13 students participated, began with the loading of the ship on September 17th at the GEOMAR pier in Kiel. Since the cabins could only be occupied once, the group of scientists on board and per leg consisted of only seven persons each. Four students each were supervised by three scientists during each cruise leg. With the installation of the gear on the work deck and the laboratories, the introduction of the students of the first cohort to the different measuring instruments also began, which was further deepened in the following days at sea. Seismic and hydroacoustic measurements east of Bornholm and the Sorgenfrei-Tornquist Zone, respectively, were aimed at studying the spatio-temporal variation of the interaction between Late Cretaceous inversion tectonics and sedimentation processes. The first cruise leg ended on September 21 in Sassnitz/Rügen. During the second leg we pursued the same scientific objectives. This leg ended on September 25th in Kiel. During the third leg we measured a tectonic fault that runs through northern Langeland and has been active since the Triassic at least up to the Neogene. Although the time spent on board was relatively short, the learning curve was very steep due to the very intensive supervision. By the end of their time on board, the students had gained a very good overview of data acquisition, processing and interpretation techniques. Last but not least, they also learned what it means to work on a research vessel. The cruise ended on September 29, 2020 in Kiel.

1.2 Zusammenfassung

Die Praktikumsfahrt AL545, an der insgesamt 13 Studierende teilnahmen, begann mit der Beladung des Schiffes am 17. September an der GEOMAR Pier in Kiel. Da die Kammern nur einfach belegt werden durften, bestand die Wissenschaftlergruppe nur jeweils aus sieben Personen. Jeweils vier Studierende wurden von drei Wissenschaftlern betreut. Mit dem Aufrüsten des Arbeitsdecks und der Labore begann auch die Einweisung der Studierenden der ersten Kohorte in die verschiedenen Messgeräte, die in den folgenden Tagen auf See weiter vertieft wurde. Seismische und hydroakustische Messungen östlich von Bornholm bzw. der Sorgenfrei-Tornquist Zone hatten das Ziel, die Raumzeitliche Variation der Wechselwirkung zwischen spät-kreidezeitlicher Inversionstektonik und Sedimentationsprozessen zu untersuchen. Der erste Fahrtabschnitt endete am 21. September in Sassnitz/Rügen. Während des zweiten Fahrtabschnitts verfolgten wir dieselben wissenschaftlichen Ziele. Dieser Abschnitt endete am 25. September in Kiel. Während des dritten Fahrtabschnittes vermaßen wir eine Störung, die sich durch das nördliche Langeland zieht und seit der Trias zumindest bis ins Neogen aktiv war. Zwar war die Verweildauer an Bord der Studierenden relativ kurz, wegen der sehr intensiven Betreuung war die Lernkurve aber sehr steil. Am Ende ihrer Zeit an Bord hatten die Studierenden einen sehr guten Überblick über die Datengewinnung, -bearbeitung und –interpretation gewonnen. Nicht zuletzt erfuhren sie ebenfalls, was es bedeutet, auf einem Forschungsschiff zu arbeiten. Die Ausfahrt endete am 29. September 2020 in Kiel.

2 Participants

2.1 Principal Investigators

Name	Institution
Hübscher, Christian, Prof. Dr.	IfG-HH

2.2 Scientific Party

Name	Discipline	Leg	Institution
Prof. Dr. Hübscher, Christian	Chief scientist	1-3	IfG-UHH
Haecker, Tobias	Tutor	1-3	IfG-UHH
Preine, Jonas	Tutor	1-2	IfG-UHH
Aster, Malte Steffen	Student	1	IfG-UHH
Dittmers, Carina	Student	1	IfG-UHH
Bogner, Laura	Student	1	IfG-UHH
Ehlies, Vanessa	Student	1	IfG-UHH
Chung, Ji In	Student	2	IfG-UHH
Lackner, Max	Student	2	IfG-UHH
Wodtke, Vincent	Student	2	IfG-UHH
Uhl, Karolina Julia	Student	2	IfG-UHH
Maaß, Regina	Tutor	3	IfG-UHH
Behr, Christian	Student	3	IfG-UHH
Devdariani, Ana	Student	3	IfG-UHH
Rehm, Alina	Student	3	IfG-UHH
Eßbach, Viktor	Student	3	IfG-UHH

2.3 Participating Institutions

IfG-UHH Institut für Geophysik, Universität Hamburg

3 Research Program

3.1 Description of the Work Area

(V. Ehlies, A. Rehm)

The work area is located at the southwest of the Baltic Sea. The location of the two main measurements lie northeast of Bornholm and southeast of Langeland. The longitude of the two islands varies about 4°E from nearly 11°E at Langeland to 15°E at Bornholm but the latitude is nearly the same around 55°N, a bit more north at Bornholm. Both islands belong to the State of Denmark. Langeland is located between Denmark and Germany and Bornholm between Sweden and Poland.

Fig. 3.1.1 Map of the western part of the Baltic Sea and the Danish Territory modified with highlighting the islands Langeland and Bornholm. Sanborns' Baltic Sea Map Page (downloaded 08.10.2020).

The geological and tectonic structures of the work area is described as follows. The Baltic Sea has gone through three phases of plate tectonics. The first phase was the compression caused during the collision of Africa, Europe and Iberia. The second phase occurred during the opening of the North Atlantic and the formation of the Alps. The last phase consists of various tectonic reactivations during the ice ages. These tectonic reactivations were caused by the loading and unloading of the ice sheets.

Starting with the Ice Ages as the age, which is literally the foundation of the Northern Basins and the coastlines and which also changed a lot of the surface nearest layers, the movement of the ground and sediments is described in figure 3.1.2. In the area of the Baltic Sea the Ice Ages took influence in the Upper Pleistocene, around 15.000 years ago.

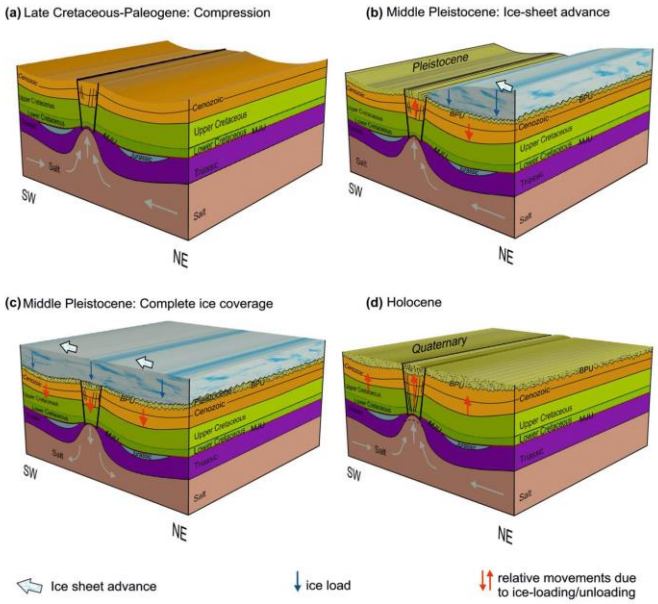

Fig. 3.1.2 Part of a 3D conceptual model modified from Al Hseinat et al.(2016) of the Cenozoic supra-salt faulting in the northern Eckernförde Bay. BPU: Base Pleistocene Unconformity; MJU: Mid Jurassic Unconformity (Huster et al., 2020).

For the upper layers of the earth's crust the ice ages are decisive. In the upper left corner (a) of the figure the compression of the first phase is shown. Here, an interference zone has formed, whereby deposits underneath can push this interference zone upwards, which can cause an offset of the earth layers. The upper right corner (b) of the figure shows the advancing ice age from northeast to southwest. The load of the ice layer pushes the deposits towards the fault, and they continue to rise there, pushing the fault further upwards. The bottom left corner (c) of the figure shows the complete cover of the fault zone covered by the ice layer. The load of the ice compresses all layers of the earth crust, as well as the fault and the deposits downwards. The bottom right corner (d) of the figure shows that the ice ages are over, and the earth layers can expand again due to the discharge of the ice layer. Thus, the deposits can raise the disturbance again.

The phases and impacts of plate tectonics are abstractly shown in Fig. 3.8.3 the tectonic map of Europe. The figure shows the major tectonic plates/terrains in different colours and the collision and structure zones as red lines. The dark red rectangle is marking the working area. It is clearly visible that the working area is right on the collision zone of Baltica (purple) and Avalonia (green). The collision took place in the early Palaeozoic, to be more precisely in the Upper Ordovician, around 440-460 Million years ago. During a collision the structure of each plate is changing. Here the change was caused by subduction and compression. The new occuring zone is named Tornquist zone.

The Alpine orogenic event started in the middle of the Mesozoic during the Middle Jurassic, around 170 Million years ago. The position is shown little in orange on the lower left sight. The larger yellow part shows the influence of the Variscan orogeny starting in the Middle Paleozoic, around 420 Million years ago.

The focus of the working area was set on the correlation of the eastern part of Glückstadt Graben, Ringkøbing-Fyn High and Tornquist zone, especially the northern part, the Sorgenfrei-Tornquist zone. The locations can be seen in figure 3.1.4 and short descriptions will follow below.

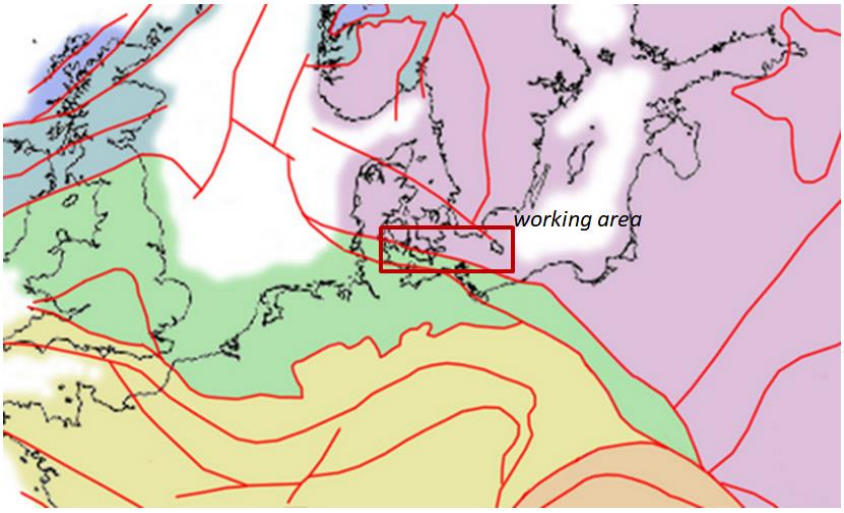

Fig. 3.1.3 Section of the Tectonic map Europe modified with a highlight of the working area. Red lines: collision and structure zones; blue: Laurentia; purple: Baltica; green: Avalonia; yellow: terrains deformed by Hercynian/Variscan orogeny; orange: terrains deformed by Alpine orogeny. Wikimedia Commons (22.06.2020).

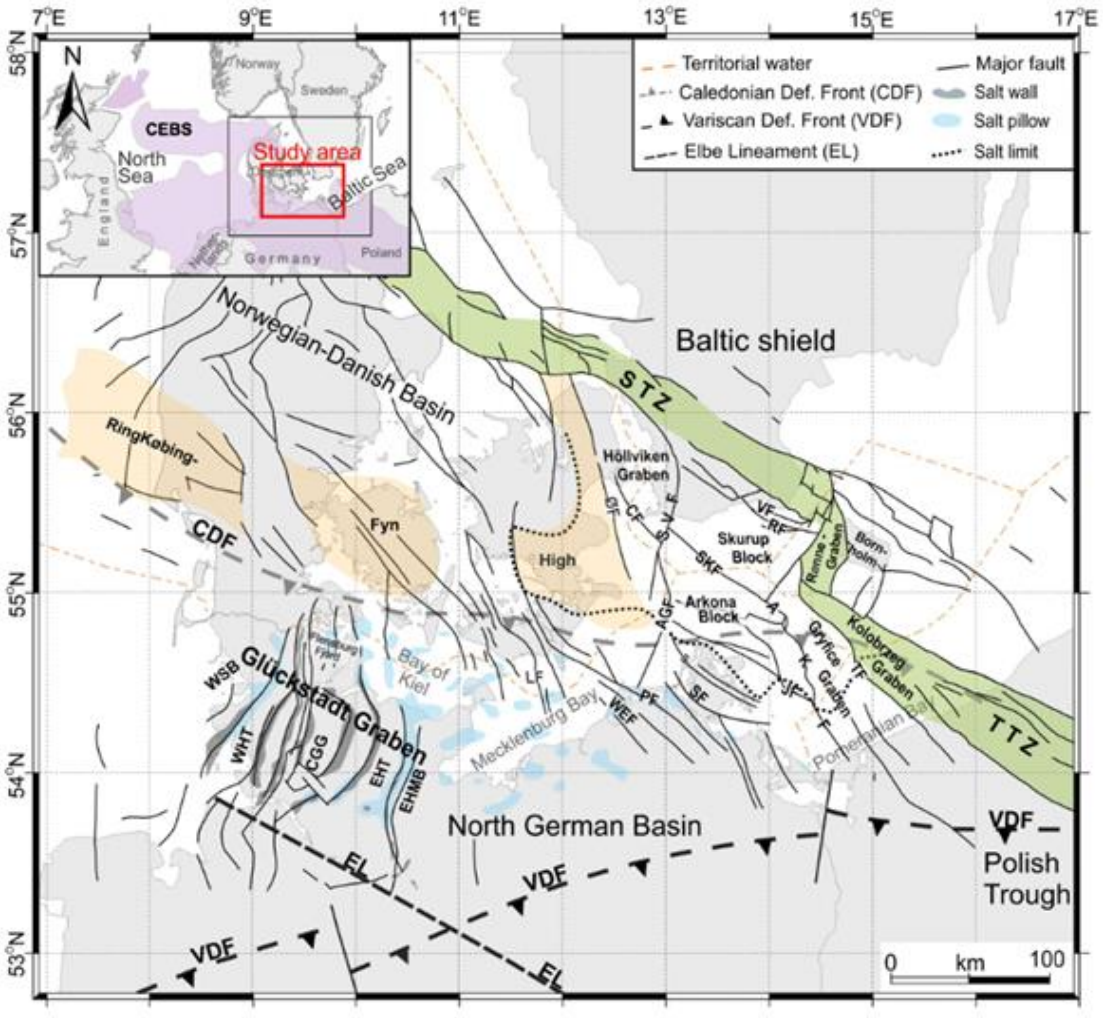

Fig. 3.1.4 Tectonic map of the Central European Basin System with the approximate location of the main structures. Modified by Al Hseinat and Hübscher (2017).

From the top to the lower right side of the figure the Tornquist zone can be seen like a green band following the pass of the deformation zone where Baltica hits Avalonia around 440-460 Million years ago. This deformation is also called Sutur and is named for the german geologist Alexander Tornquist. It is separated into two parts, the north-western part, the Sorgenfrei-Tornquist zone (STZ), and the south-eastern part, the Tesseyre-Tornquist zone (TTZ). Both are separated after another fault shifted the TTZ down south, caused by the Alpine orogenic event starting around 170 Million years ago during the Middle Jurassic.

In the middle of the figure between Glückstadt Graben and Tornquist zone, shown in light red, is the Ringkøbing-Fyn High. Its origin is caused by the Tornquist zone and the thinner and younger layers in front of this deformation. The age is estimated in the Mesozoic during the Lower Triassic around 250 Million years ago. Nowadays it is located in the south of the Danish Basin and covers the Danish territory Jutland and the Danish islands in the Baltic Sea. The main structure is described as a crust-high layer.

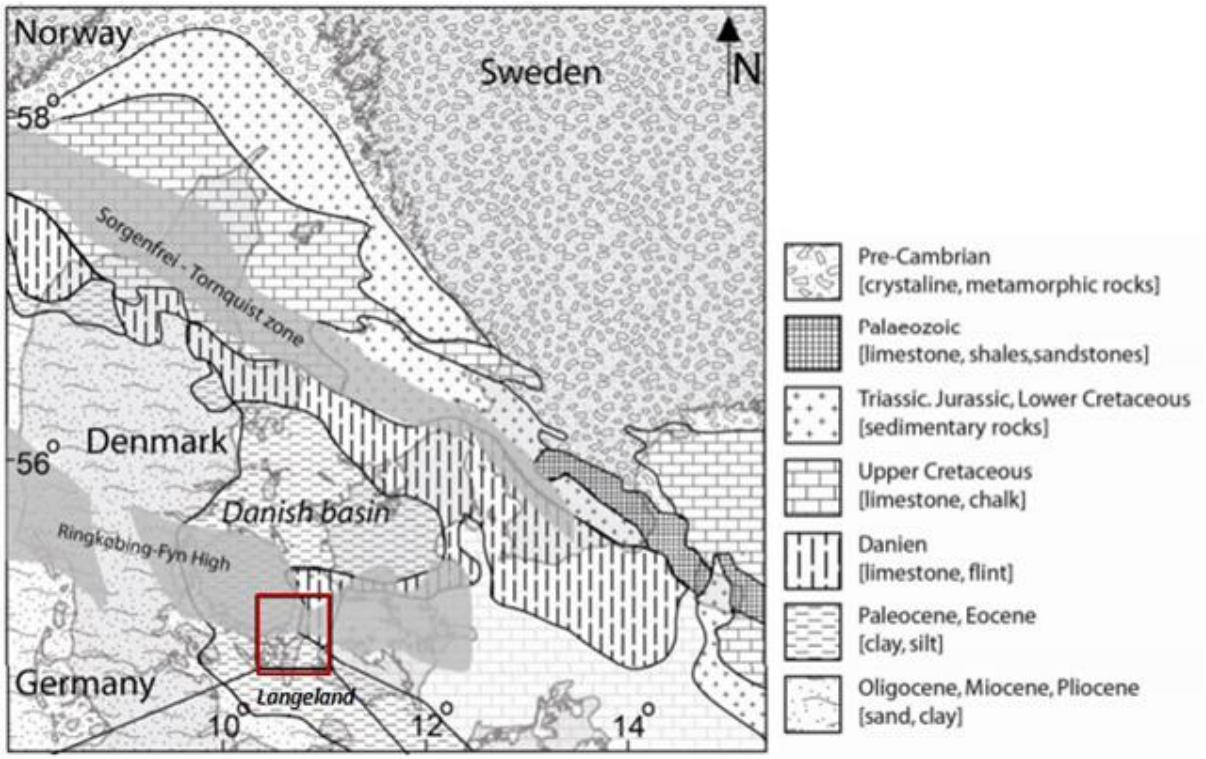

Fig. 3.1.5 Map of the geological setting in the Danish basin. Modified with highlighting Langeland. Compiled by Andersen et al. (2016).

All of the phases and the impacts explained above can be described in the example of the geological history of the island Langeland (Fig. 3.1.5). It is located south in the Danish basin right in the Ringkøbing-Fyn High. The island has grown out of the collision and opening of the tectonic plates. Furthermore the phase of the Ice Ages and the glaciers occurred the sedimentary deposition and the structure of the ground.

Former measurements have shown, that the geologic structure is dominated by sand, clay and limestone. Especially a Danish national groundwater mapping campaign initiated in 1998 generated a geological profile formed by AEM data and boreholes, as seen in Fig. 3.1.6 A. In addition to that geological profile the model formed, the data has also been interpreted for

resistivity and thus for the conductivity. In Comparison part B represents the conceptual geological profile through the northern part of the island, showing the distribution of the layers and on the same position a cross section, part C, points out the location of a fault going through the northern part of Langeland. The interpreted geological model is shown in part D.

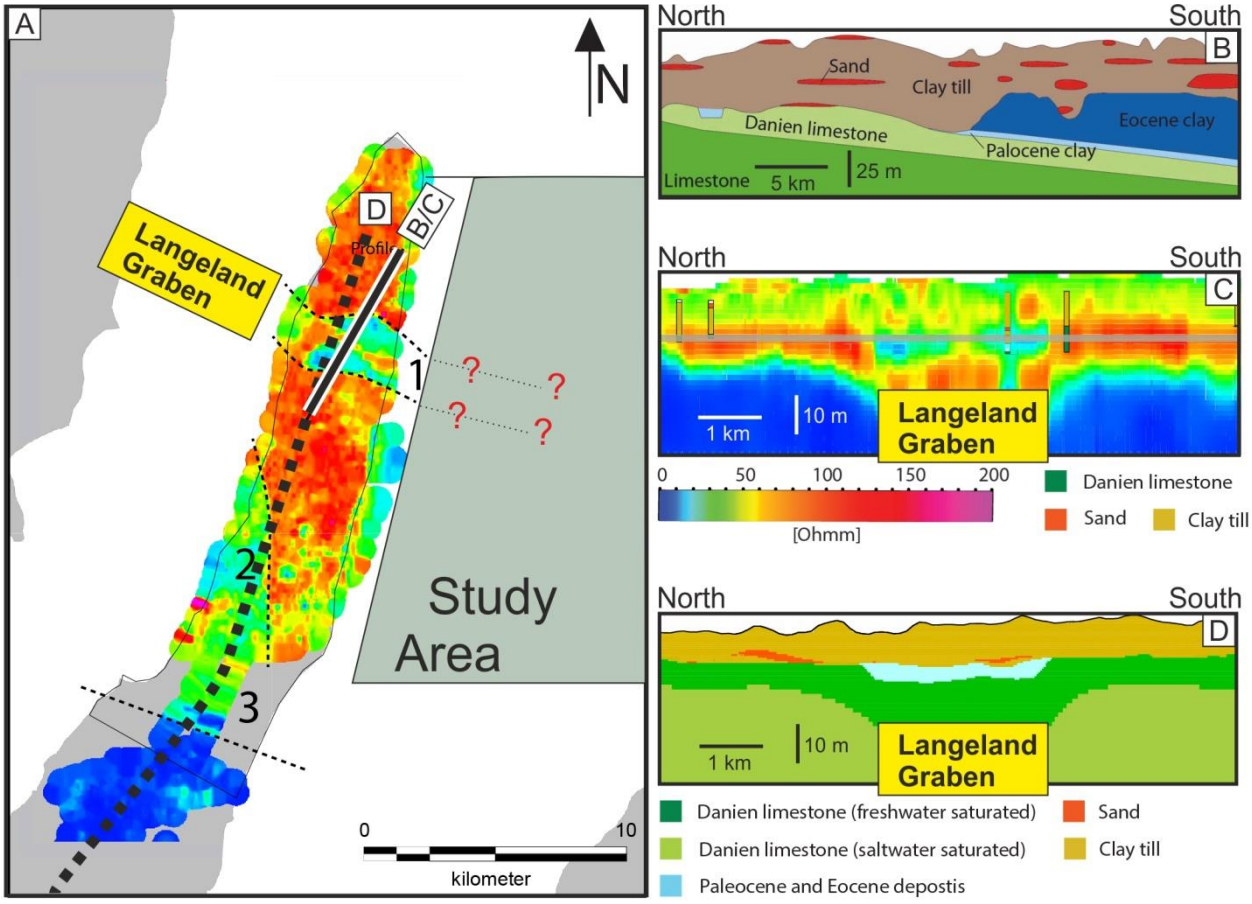

Fig. 3.1.6 Resistivity map and cross section of the northern part of Langeland . Interpreted by Andersen et al. (2016). A) Mean resistivity map at the elevation -25 m. B) Conceptual geological profile through the northern part of Langeland. C) Cross section through the northern fault system with the presence of AEM data and boreholes. The elevation of the mean resistivity map is shown with the grey line. D) Interpreted geological model.

Another measurement in 2016, a reflection seismic study, shows the layers in an interpreted seismic section northeast of Langeland in figure 3.1.7. The layers from top to bottom are seperated into the ages Pleistocene, Tertiary, Cretaceous, Jurassic and Triassic. The structure is formed by the faults, here pictured in black lines.

In a conclusion it can be stated that the work area is characterized by the structures and events described above. As there are still recent activities and extant tectonic events, the structure and faults might still change and former measurements might already look different because of this fragile deformation zone.

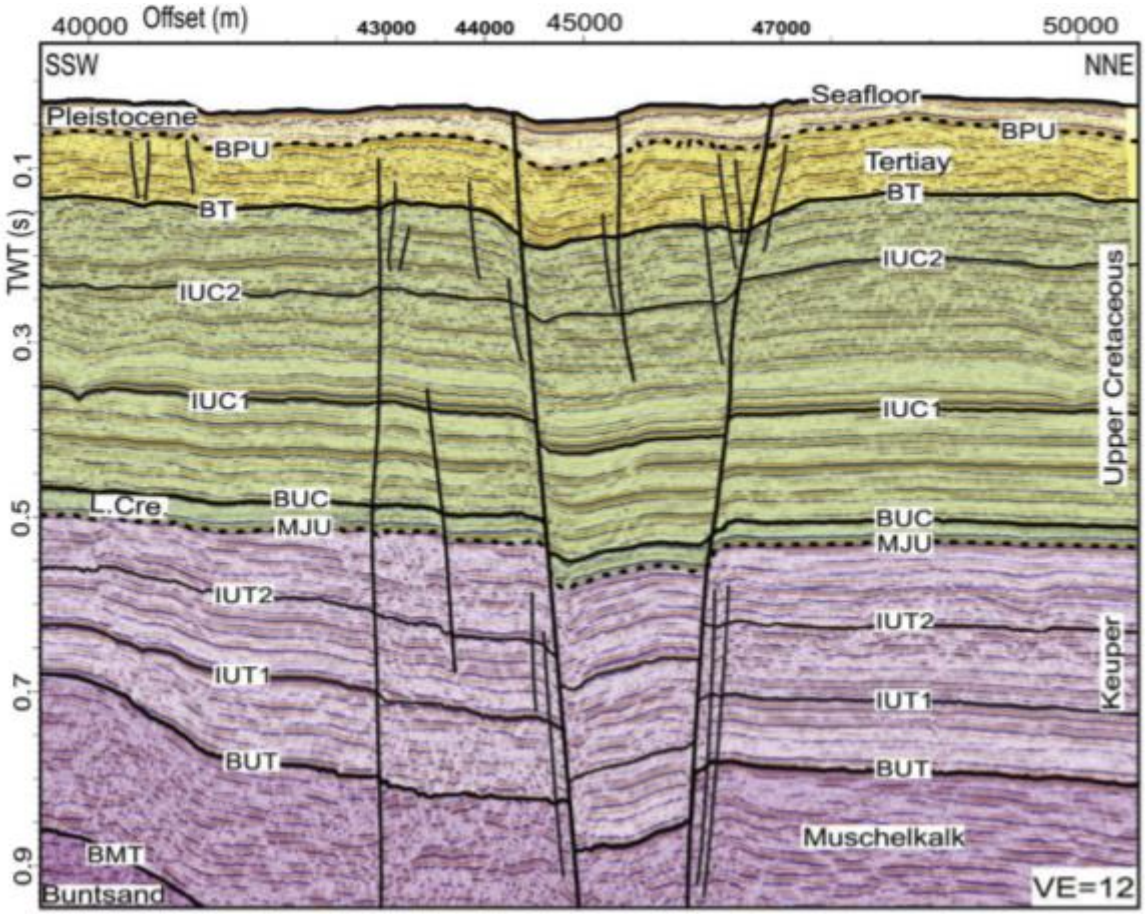

Fig. 3.1.7 SSW-NNE time-migrated/interpreted seismic section northeast of Langeland. Black lines mark fault systems. BMT: Base Middle Triassic; BPU: Base Pleistocene Unconformity; BT: Base Tertiary; BUC: Base Upper Cretaceous; BUT: Base Upper Triassic; IUC 1 and 2: Internal Upper Cretaceous 1 and 2; IUT 1 and 2: Internal Upper Triassic 1 and 2; and MJU: Mid Jurassic Unconformity. Modified by Al Hseinat and Hübscher (2017).

3.2 Aims of the Cruise

(C. Hübscher)

In the course of the field exercise and in order to fulfil the pretention of combining education and research the student participants learn

- to install deck gear and lab instruments in accordance with safety instructions,
- to calculate a daily schedule, to communicate plans with the bridge,
- to prepare, maintain, deploy and retrieve a seismic source and a marine magnetometer/gradiometer,
- to process reflection seismic data with VISTA processing software (CMP-binning, bandpass filtering, gain, velocity determination, stack, poststack-time migration),
- to interpret collected data in terms of cruise specific scientific aims,
- to behave correctly in a closed, special working environment like a research vessel.

In order to demonstrate a research cruise, the following scientific objectives were selected:

- Interaction between cretaceous inversion tectonics and bottom currents and sedimentation in the Baltic sector of the Sorgenfrei-Tornquist Zone north-east of Bornholm.
- Mapping of the Langeland fault.
- Imaging of current controlled sediment features in the Langeland Belt.

3.3 Agenda of the Cruise

(C. Hübscher)

The cruise started and ended in Kiel (Fig. 3.1).The training of the students comprised several aspects. On deck, the preparation, deployment, recovery and maintenance of pneumatic seismic sources such as the GI-Gun was one center-piece of the technical training. The students learned how to disassemble the device, to clean, grease and reassemble it. In the lab, the student did regular shifts 24/7. They were 4 hours on duty with an interruption of 8 hours. During the watch free time we continued with lectures on the instruments and data processing. Watch keepers monitor the reflection seismic, magnetic and parametric echosounder systems. Beside the monitoring we taught data processing with a strong focus on seismic data processing with Schlumbergers VISTA seismic processing software. The students set-up the geometry (CMP-binning), they determined bandpass filters in dependence of the seismic source, the found an appropriate gain and do a velocity determination. After the stack, a post-stack time migration was applied. Time migrated brutstacks are available of almost all profiles at the end of the cruise. Each late afternoon the entire group met at the science meeting and we discussed the profiles of the last 24 hours. Underway findings were used to adapt the profile layout. Measurements have been carried out around Bornholm and east of Langeland (Fig. 3.3.1).

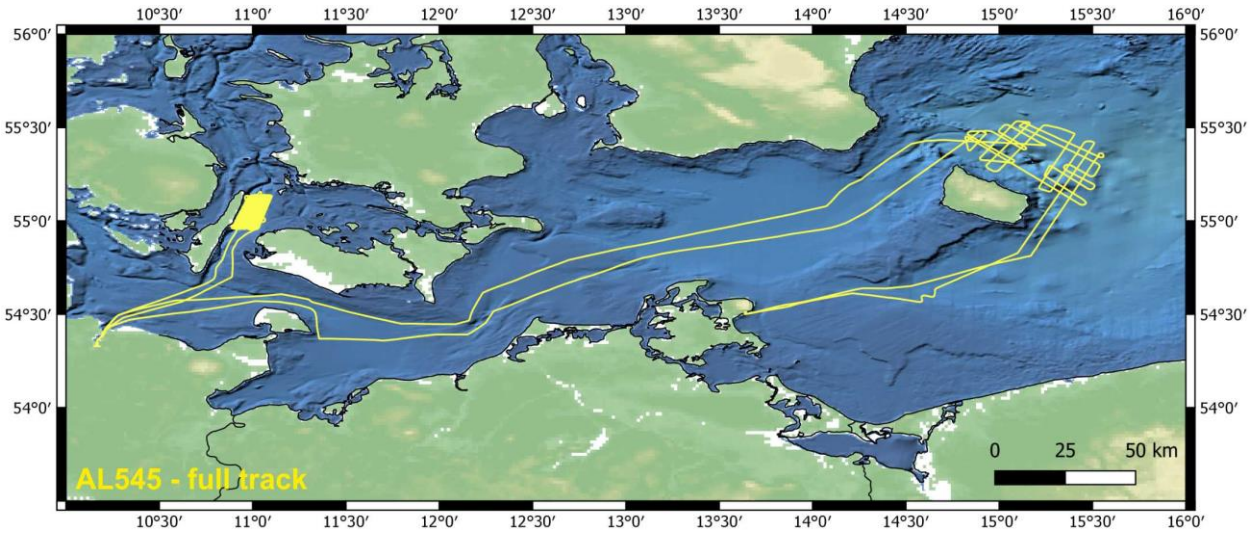

Fig. 3.3.1 Track chart of R/V ALKOR Cruise AL545. Bathymetry from EMODNet.

4 Narrative of the Cruise

(C. Hübscher, T. Häcker, J. Preine)

The AL545 Scientific Party of seven scientists arrived at RV ALKOR at the GEOMAR Pier on September 17 19 at 11:00, where they unloaded the equipment from a truck and started with installations on deck and the labs. Owing to the COVID-19 pandemic the entire scientific party comprised only seven persons, four students, two tutors and the chief scientist. The RV ALKOR departed from Kiel in the morning of 18 September and began her transit to Mecklenburg Bay. Between 09:00 and 10:30 the junior participants participated in the mandatory security introduction and a tour around the ship, during which all safety equipment and safety measures were explained by the chief mate. The transit ended at 13:00 east of Fehmarn, where two MicroEel streamers and a Mini-GI seismic source were deployed. Since no marine mammals were detected during the mitigation period, the low energy seismic source was released the first time. The following two hours were used to optimize the Injector delay, trigger interval and streamer setup. At 16:15 all gear was put back on deck, and the vessel started its transit towards Bornholm. The evening was used for a summary talk in which the scientific goals of the cruise were summarized.

In the morning of 19 September at 08:00 the deployment of the seismic gear and the marine mammal mitigation started. After a short instrument test and a soft start of the seismic source measurements along the first seismic profile across the Sorgenfrei-Tornquist Zone started. Based on some test shots the seismic processing flow was determined by the tutors. In the afternoon, the student participants got a thorough introduction into watch keeping duties, which included seismic processing. Profiling continued until September 21. After lunch, all towed gear was put on deck and the vessel transited to Sassnitz (Rügen) harbor, where RV ALKOR arrived at 16:00. Four students disembarked and were replaced by four newcomers. The evening was used for a first introduction into the rules on board, the scientific installations, and a wrap up of scientific findings during the first cruise leg.

The vessel left Sassnitz harbor on September 22 at 08:00. The safety introduction was held at 09:00 during the transit back to the Bornholm area. After arrival early afternoon, the seismic equipment as well as the marine magnetometer was deployed and the scientific profiling commenced. Several profiles perpendicular to the local dominant tectonic fault systems provided insight into the interaction between inversion tectonics and sedimentation. Cross profiles helped to link the seismic stratigraphy between the individual profiles. These measurements lasted until September 24 10:20, when all towed gear was recovered. Around noon, the transit to Kiel started.

The second leg ended on September 25 at 08:00 a.m. when the ship docked at its pier on the west coast of the Kieler Förde. Five students disembarked and the remaining scientists and crew welcomed the five newly arrived students. The transit to the working area east of northern Langeland started one hour later and lasted until 13:30. The transit was used for safety instructions and first introductions into the installed scientific gear. Profiling commenced at 15:00. Altogether 26 profiles were collected in the eastern prolongation of a West-East striking, Pleistocene and possibly fault controlled graben in northern Langeland. The data processing flow for the seismic data was refined. Underway data processing was in full swing early next day. The working program was fulfilled on September 28 at 11:00. All gear was recovered and placed on

deck and the transit back to Kiel started. The data processing was continued while all scientific devices on deck were disassembled into their components before packing. RV ALKOR arrived the EOMAR pier at 17:00, when the last boxes were stowed away and lashed. On September 29 all equipment was unloaded and the scientific crew disembarked – AL545 was over.

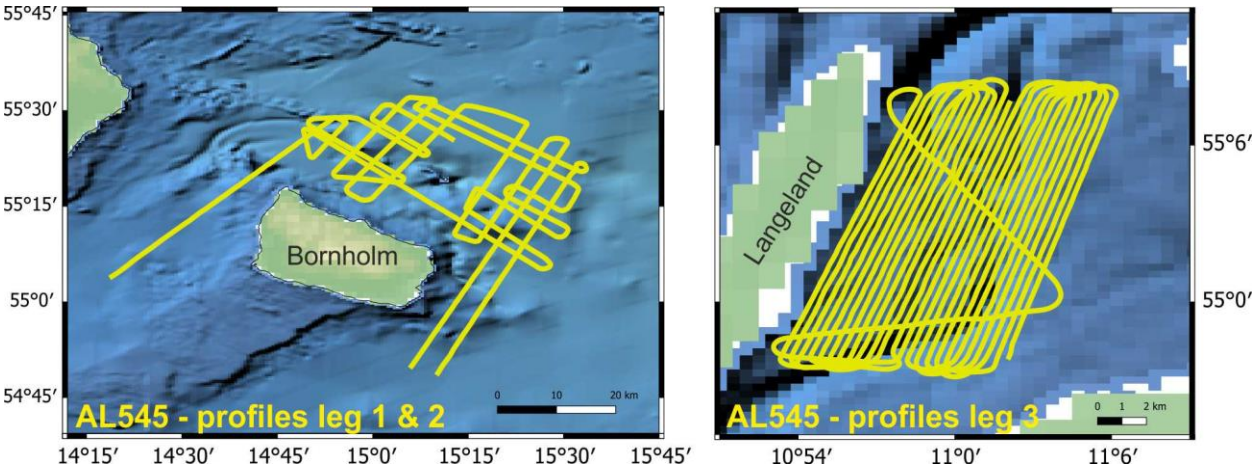

Fig. 4.1 Geophysical profiles of AL545 cruise.

5 Preliminary Results

5.1 Underway Hydroacoustics

(L. Bogner)

5.1.1 Multibeam Echosounder

The Multibeam Echsosounder works based on the backscattering of energy. The sound waves reach the oceans bottom, but do not get reflected back to the receiver, because the angle with which it is sent out is too big. The moment the wave reaches the bottom, there is however energy that gets scattered and is now partially reflected back to the receiver. The strength of the signal is dependent on certain characteristics. First to be considered is the angle in which the signal reaches the bottom. The narrower the angle, the more energy can be scattered back. Secondly the roughness of the ocean floor is of importance, as different objects that lie within the wavelength of the signal can cause the backscattered energy to be bigger or smaller. For example, the rougher the surface is that is to be surveyed, the more energy will be scattered back. The third influential factors are specific properties of the bottom surface. If the waves are slightly entering the ground, the angles of the backscattered energy can be altered.

The Multibeam Echosounder is mainly used for Bathymetry, thus for measurements of the ocean floor. The main goals we want to reach by using this method are to calculate 1st the depth through the two way travel time and 2nd the roughness of the seafloor through the amplitudes of the backscattered energy.

The Multibeam Echosounder is located at the hull. It consists of a transducer, which produces many beams. Each of those beams has a different angle in which the signal is emitted, forming the shape of a fan. This fan usually has an altogether opening angle that lies between 120° and 150°, which implies it crosswise covers up to 7,4 times the current depth. Thus the width of the surveyed sea floor is dependent on the current depth as well as on the opening angle of the fan. The two way travel time is measured to calculate the current depth. To obtain correct results, the

varying density and therefore the breaking of the soundwaves in the water column has to be corrected by a velocity model. This is a complicated process but delivers a precise determination of the water depth.

5.1.2 Parametric Echosounder

For sub-bottom profiling sound pulses are transmitted to the seafloor. These pulses are reflected at the seafloor, at sediment layers and objects. Therefor the sound pulse is created at a transducer at the hull, which is received by the transducer as well. The system measures the two-way-travel time of the reflected signal. By a real time, signal processing the received data is evaluated on board to get first survey results immediately. Caused by rough sea the transducer may move during the survey in 6 directions. The most important unwanted motions are roll, pitch and heave. They should be compensated, if high-resolution echo prints are required.

We have used a parametric echo sounder, so it's helpful to describe the parametric effect shortly. First two signals of slightly different high frequencies at high sound pressures are transmitted. Because of non-linearities in the sound propagation at high pressures both signals interact, and new frequencies are arising, for example the so-called difference frequency which we use for our survey. The advantage of the low frequency is a greater penetration depth within a smaller transducer dimension caused by the parametric effect.

The particular system which was in use is a SES 2000 deep from the company Innomar. The working frequency was 6 kHz. Furthermore, the data in the first leg was recorded over a length of 80 m which depends on the actual seafloor depths. A maximum depth of 130 m was recorded. In the second leg the data was recorded over a length of 100 m, so our recorded data was mostly between 40 m and 310 m. While recording the longitude and latitude where saved on SIS 1 and 2, the time and date on SIS 3 and 4 and a last the UTM coordinates at SIS 5 and 6. To finally work with the data, we converted the RAW format into SEG-Y format to use it in the processing.

5.2 Multi-channel Reflection Seismics

5.2.1 The Marine Seismic Source

(A. Devdriani, C. Behr)

To collect the seismic data as efficiently as possible a geophysicist should know exactly what to look out for while choosing the equipment with (usually) tight budget. Which are the important and not-so-important factors that lead to the final results.

The typically used source for marine seismic are air guns. They generate a pressure pulse by expelling a fixed volume of compressed air underwater. The characteristic sound produced when the gun fires is called its pressure signature and it has three main components: 1) The direct arrival - the sound produced when the air gun's ports first open; 2) The "source ghost" - the energy pulse which travels upward from the gun. It is almost perfectly reflected from the sea surface. 3) The bubble pulses produced by the expansion-collapse cycle of the air bubble created in the water when an air gun fires. The important properties of an airgun's signature are characterized by three parameters: strength, which is the amplitude of the sound, measured at the direct arrival's peak (peak strength) or from the direct arrival's peak to the ghost arrival's peak (peak-to-peak strength (PTP)), primary-to-bubble ratio (PBR), which is the peak-to-peak strength of the direct arrival divided by the peak-to-peak strength of residual bubble pulses and

bubble period, time between consecutive bubble pulses. Another important parameter, which does not depend on the gun itself, but on how it is deployed, is the frequency spectrum.

For applications, where the aim is to get a high amplitude signal e.g. researching the oceanic crust, it is a common misconception to assume that gun volume, which is the typical volume of air expelled after firing a single air gun, has a big impact on the amplitude of the sound. In reality, the peak strength of an air-gun's signature is proportional to the cube root of the gun's volume. E.g. After doubling the volume of all guns in an array its peak strength will be increased by less than 26%, because some of the potential strength gain is lost due to increased interactions of larger air bubbles (Dragoset, 1990). Another common misconception is thinking gun parameter categories, such as firing pressure, port area, and port closure pressure are crucial in attaining some particular spec goal. All three parameters affect the strength or shape of an air gun's signature, but only weakly (Dragoset, 1990)

On the other hand, the amplitude of the signal is roughly proportional to the number of guns. That's one of the reasons tuned air gun array concept is being used, in which many guns are fired simultaneously. That way direct arrivals from individual guns sum coherently below the array and produce a much louder sound than that from a single gun. Arrays are typically located 5-10 m below the sea surface, so that guns will fire below the surface of the water. If guns are bobbing in and out of the water as they fire, energy transmitted into the earth will be quite variable; especially if guns fire above the surface.

For applications, where the bandwidth is the main concern, one should carefully choose the towing depth of the source, because this relates to the position of the so called "ghost notches" in the frequency spectrum. These ghost notches are caused by the destructive interference between the direct signal and the time delayed ghost signal. The time delay of the ghost is proportional to the towing depth of the source. The ghost notches are positioned at frequencies, for which the time delay equals multiples of oscillation period. So, the deeper the source is towed, the lower is the frequency of the first notch. Conversely a shallow source has a large signal bandwidth, but has a much weaker low-frequency response than an array towed at standard depth. In other words, putting guns shallower diminishes the amplitude of the signature at all frequencies below 100 Hz, in this case by an average of about 6 dB.

For measurements with the aim to resolve small structures, it is more important to have a large bandwidth rather than a high signal amplitude, therefor it is preferable to deploy the source as shallow as possible without risking to have it fired above the water. On the other hand for measuring structures deep in the crust, it would be preferable to deploy the source relatively deep, to avoid amplitude losses in the lower frequencies, since these are better able to reach deeper structures.

The residual bubble pulses are usually considered as noise and their reduction is always desirable. There are two approaches for this: arraying guns with different bubble periods and the GI-gun. When simultaneously firing multiple air guns with different bubble periods, the direct signals add up coherently, while the bubble pulses add up incoherently, which increases the PBR compared to that of a single gun. The GI-gun consist of two air guns, one of these is called Generator, while the other is called Injector. The Generator functions as a normal air gun to produce the signal. The Injector releases its air delayed into the expanded bubble and thus reduces the collapse of the expanded bubble and the bubble pulse.

For choosing a source for a given application, one also has to consider, that an expanded source creates an anisotropic signal. Since the signal incorporates the reflection at the surface of the water, even a single air gun has to be considered as an expanded source. In this case the time delay of the ghost signal and therefor also the frequencies of ghost notches depend on the angle between the viewed direction and the vertical axis of the source. This also applies to every air gun of an array, but in this that angle also affects the simultaneity of the direct signals and thus the amplitude of the combined signal.

Other factors that do matter are mechanical reliability, signature stability, ease of deployment, towing stability, the number of guns a crew can fire, crew availability and crew costs. In other words, achieving optimal results with tight budget is possible, one should just know what to pay attention to.

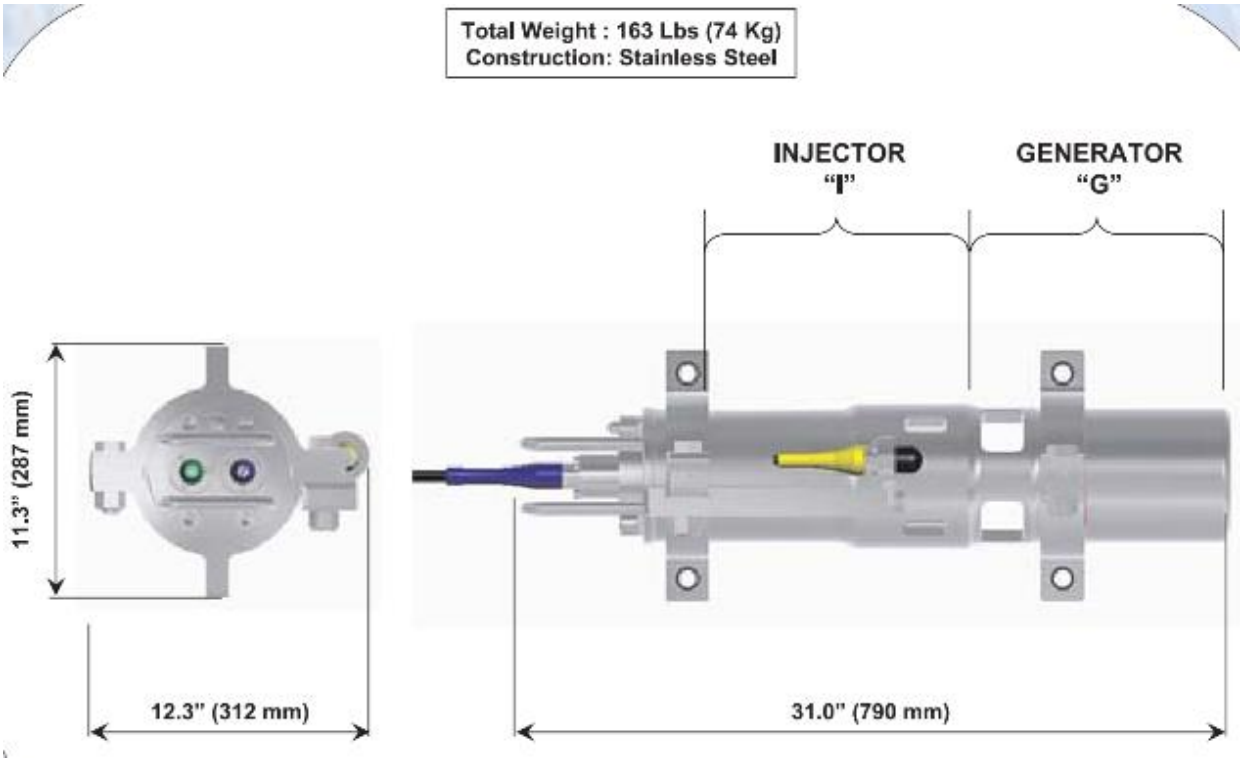

Fig. 5.2.1.1 The GI-Gun (Manual provided by SERCEL).

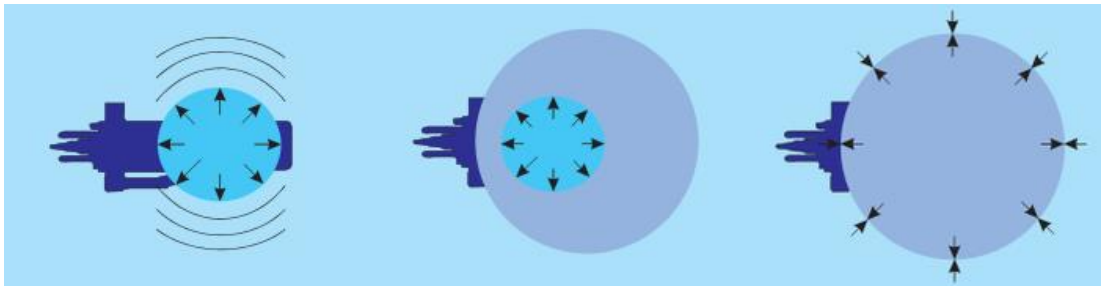

Fig.5.2.1.2 The picture shows the 3 phases in firing a GI-Gun: firing the Generator, firing the Injector and reduced bubble collapse (Manual provided by SERCEL).

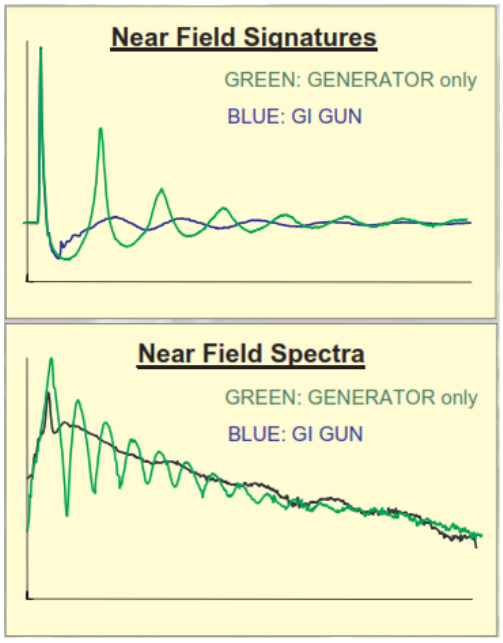

Fig.5.2.1.3 Near Field Signatures and Spectra comparison (Manual provided by SERCEL).

5.2.2 The seismic streamer

(Max Lackner)

Streamers are used in marine seismic. They are towed by vessels and receive reflected signals, which are sent from an airgun, which is positioned between the vessel and the streamer. A Streamer is a measuring hose with hydrophones. Those hydrophones convert the sound waves into electric currents, which are transferred to the vessel, where it gets processed. While measuring, the vessels travels with a speed of about 5 knots, which is around 9 km/h. This speed is used because it's a good compromise between progress and noise pollution. Streamers can have lengths between 100 and 20.000 meters. The shorter ones are usually used by research vessels close to shores. The longer ones are used by the carbon oxide industry, to find new resource deposits. Seismic streamers are using the principle of seismic reflection, which gives information of the structure of the earths shell and its components.

The general building blocks of a streamer are:

1. The deck cable connects the streamer and geodes on the vessel.
2. The lead-in is used to tow the streamer. The distance between the vessel and the streamer is determined by the length of it. It shouldn't be too short, to minimize the noise pollution of the engine.
3. The stretch-Section is an elastic element, which absorbs the acceleration of the vessel/the boi at the end of the streamer.
4. The active section is the longest element and contains the hydrophones. The hydrophones are placed in groups which build a so-called channel.
5. Birds may be used to keep the hole streamer at a consistent depth. Those birds can rotate freely and use wings to steer. The angle of the wings can be changed, to create down/up-forces. These angles are controlled by depth-sensors, which measure the hydrostatic pressure. The entire streamer is not always in a straight line behind the vessel, which is caused by currents. To get to know the exact positions, every bird contains a compass.

6. The end of the streamer is marked by a buoy. It serves as a visual signal for other vessels.

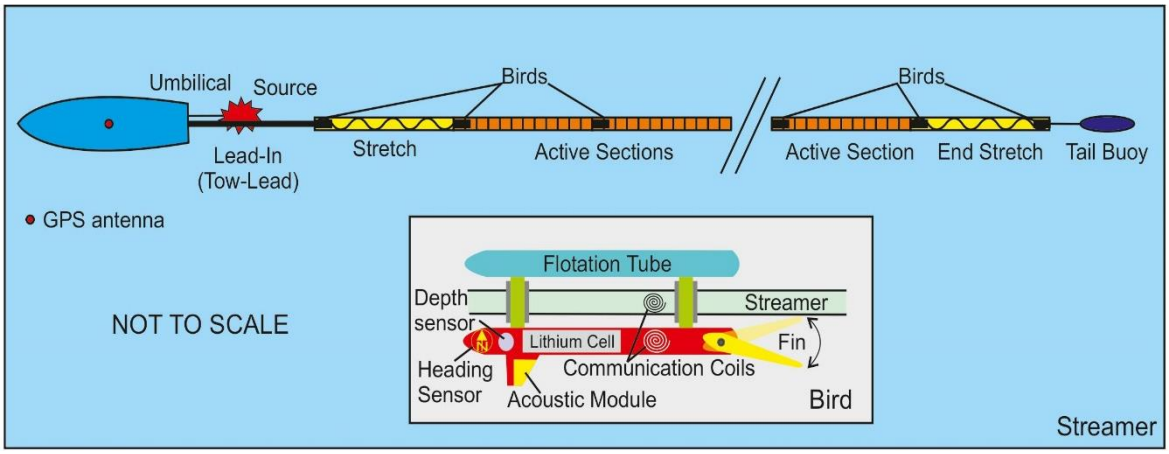

Fig. 5.2.2.1 Streamer design (after Hübscher und Gohl, 2014).

Hydrophones convert the sound waves into electrical currents. The piezoelectric effect is used for this conversion, which happens in piezoelectric thickness oscillators. A piezoelectric thickness oscillator converts pressure changes proportional into alternation Current (AC). In the built-in piezoelectric elements are materials, which generate electric currents, when mechanical pressure is applied. Through the frequent changes of mechanical pressure, dipoles in the same frequency as the sound waves are generated. This generates a AC. Common materials for piezoelectric thickness oscillators are PZT-ceramics and PVDF-foil. PZT-ceramics have a density of 7.5g/cm3, a sound wave velocity of 4600m/s and a broadband receiver goodness of 90, which implies, that almost every frequency can be recorded. Because it is used in very thin layers, which are fragile at high pressure changes, it is mostly used in echo-plus systems. PVDF-foils have a density of 1.78g/cm3, a sound wave velocity of 2260m/s. The low density implies a high absorption and a low broadband receiver goodness of 15, which implies, that only a few frequencies can be recorded. That way PVDF-foils additionally work as a low-pass filter. Furthermore, the density and the sound wave velocity are close to the ones from seawater, which results in high acoustic linking. This material is robust until a thickness of a few micrometers. This an advantage because a low thickness implies an increase of the data quality.

An acceleration compensating hydrophone compensates the acceleration of the streamer in the direction of travel. That way it doesn't have to be done in processing. In those hydrophones two piezoelectric plates are positioned parallel to the direction of travel. The plates are positioned reversed to each other, positive-and negative poles are face to face. The sum of acceleration is now zero. The vertical signals (sound waves) are not affected.

Example: The ghost signal, which is phase reversed and reflected on the water surface comes from above and the primary (and secondary...) signal comes from below.

A streamer contains multiple hydrophone groups. The number and distance between the hydrophones directly affect the signal-noise ratio und that way the solution of the end product as well. The law of big number implies that more hydrophones and more hydrophone groups imply a better result. But it must be considered that longer hydrophone groups deliver higher frequencies, which is caused by destructive interferences. These destructive interferences are

caused by the run time differences between the first and the last hydrophone of each group. This difference shouldn't be bigger than 1/4 of the dominant sound wavelength. So, the maximum hydrophone group size is already determined at the construction of each streamer. The other affecting parameters are part of the spatial response function, which result shouldn't be smaller than 0.7(-3db).

The optimal hydrophone group length is dependent from frequency characteristics of the seismic signal and the distance between the signal origin and the hydrophone/angle alpha at the point of reflection. This leads to hydrophone groups with various lengths. To uncomplicate this, nowadays every hydrophone is recorded on its own. The hydrophone groups are determined later in the data processing.

The towing depth is affected by multiple parameters. The density of the streamer is the most important one, which usually matches the density of water (1g/cm3). Because most of the technical parts, like the hydrophones, are much heavier than this, the filling material got a lower density of approximately 0.9g/cm3. Light plastics, like polyurethan, are common materials. Furthermore, the birds and the speed of the vessel can influence the depth. The faster the vessel is, the more up force is created. The only natural parameters are currents and changes in the water density, which are caused by salinity/temperature changes. The signals, which the hydrophones receive can be influenced by noise, like wave acoustics and interferences. To counter that, the streamer shouldn't be too close to the water surface and not in an area, where destructive interferences are present. This area is dependable on the ghost signal, which should overlap itself. This happens at exactly 1/4 and 3/4 of the sound wavelength. Usually the depth of 1/4 is used, because the ghost signal and the primary signal should temporally be as close together as possible, to simplify the processing.

5.2.3 Geometry of Towed Equipment

(M. Aster)

Due to structural conditions the airgun and the two streamers could not be aligned in a straight line. The three components were attached to the hull side by side (see figure 1). As a result, the geometry or the towed equipment had to be calculated so that the offsets of each hydrophone could be registered in the program.

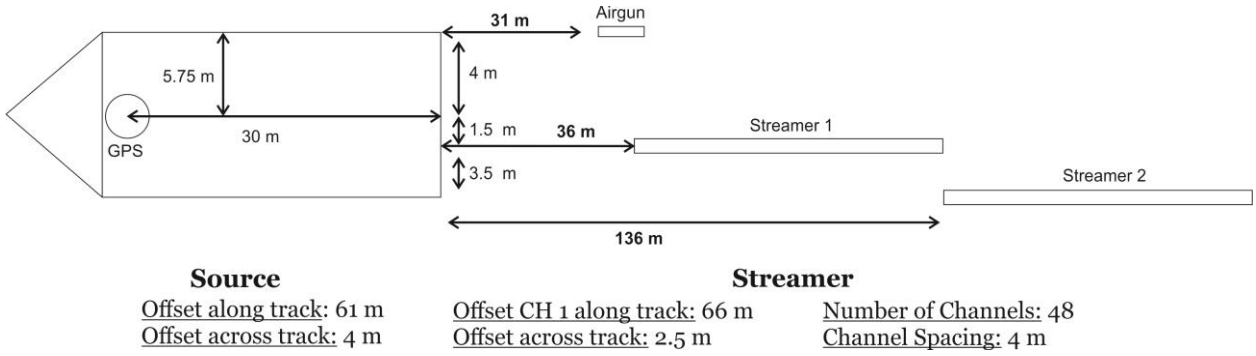

Fig. 5.2.3.1 Sketch of the geometry of the towed equipment.

At first a shot gather was used to determine the first arrival of the direct wave of the direct wave. The value of the time was picked and entered in a table for further calculation. With help of these values the offset of each hydrophone could get calculated. The speed of sound in the water was assumed as 1500 meters per second. This results in following formula: d = 1,5 * t; t: first arrival in ms.

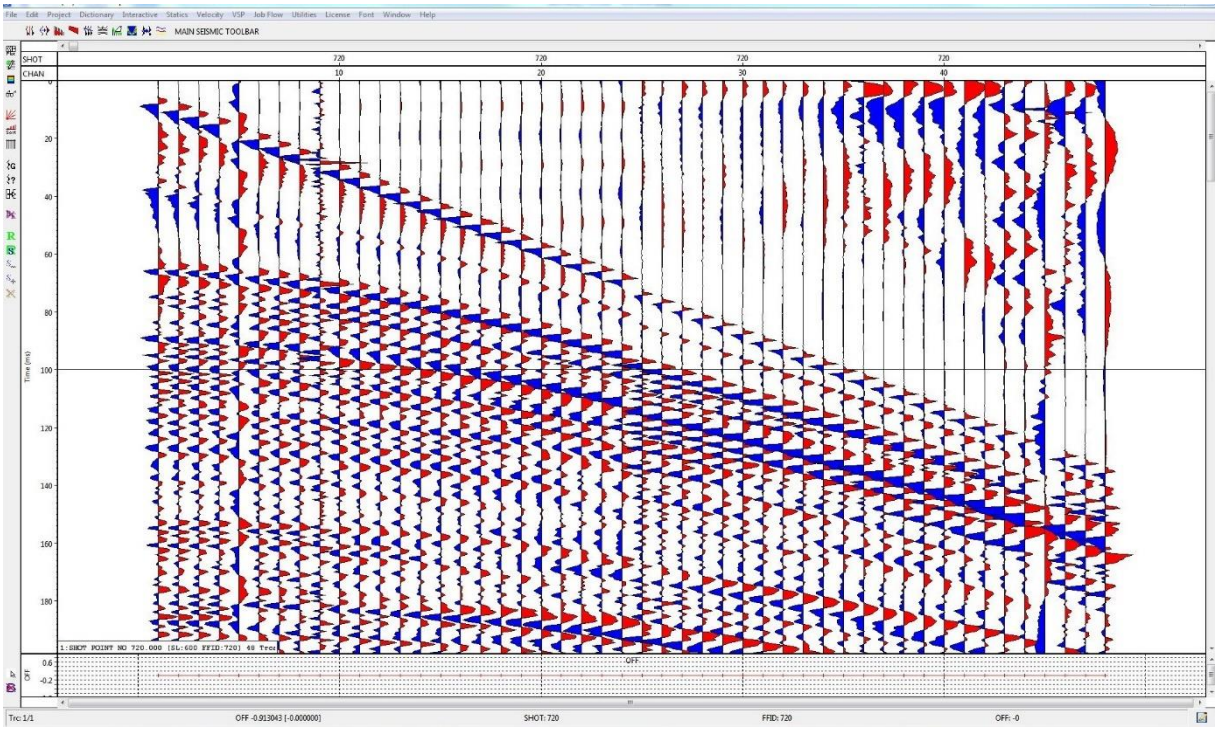

Fig. 5.2.3.2 Shot gather. First arrival times of the direct wave were picked by hand.

Subsequently the distances between each of the hydrophones were calculated with this data. In table 5.2.3.1 a few values are shown as examples. There is an unusual big time interval between channel 24 and 25. This is the result of having two streamers aligned side by side. It was technically impossible to adjust the two streamers with a precision which led to a gap between the first hydrophone of the second streamer and the last hydrophone of the first streamer with the same length as the difference between two hydrophones in one streamer. The median of the difference between two hydrophones is 3,945 m for the first streamer and 3,915 m for the second streamer. This matches well with the actual value of 4 m.

Tab. 5.2.3.1 First arrival times of the direct wave and calculated offsets and differences between the hydrophones

Channel	Time [ms]	Offset (1500 m/s) [m]	Difference (1500 m/s) [m]
1	6.07	9.11	
4	13.08	19.62	3.81
8	23.61	35.42	3.86
12	34.26	51.39	3.98
16	45.12	67.68	3.94
20	55.98	83.97	4.31
24	66.57	99.86	3.75
25	72.06	108.09	8.24
28	80.19	120.29	3.91
32	90.82	136.23	3.91
36	101.17	151.76	3.58
40	112.11	168.17	4.36
44	121.94	182.91	2.97
48	133.56	200.34	3.92

5.2.4 Seismic data processing

(V. Essbach, R. Maas)

When seismic measurements are conducted, the hydrophones that are fixed in the streamers deliver an analogue alternating current. This signal has to be digitalized to allow for further processing. To do so, the current is measured in discrete intervals, and the values are transcribed to raw data files. Certain principles have to be adhered during this step to prevent the misidentification of the analogue frequencies. For example, an electric signal of 25 Hz that is sampled every 0.01 seconds (or with a frequency of 100 Hz) can be reconstructed definitely from the data (Figure 5.2.4.1).

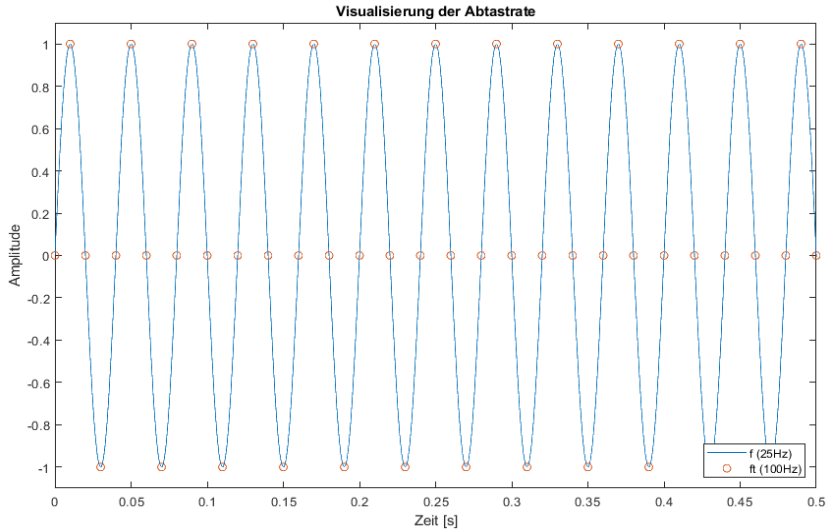

Fig. 5.2.4.1 Example for an electric signal that is fully recovered (blue: real signal, red: data).

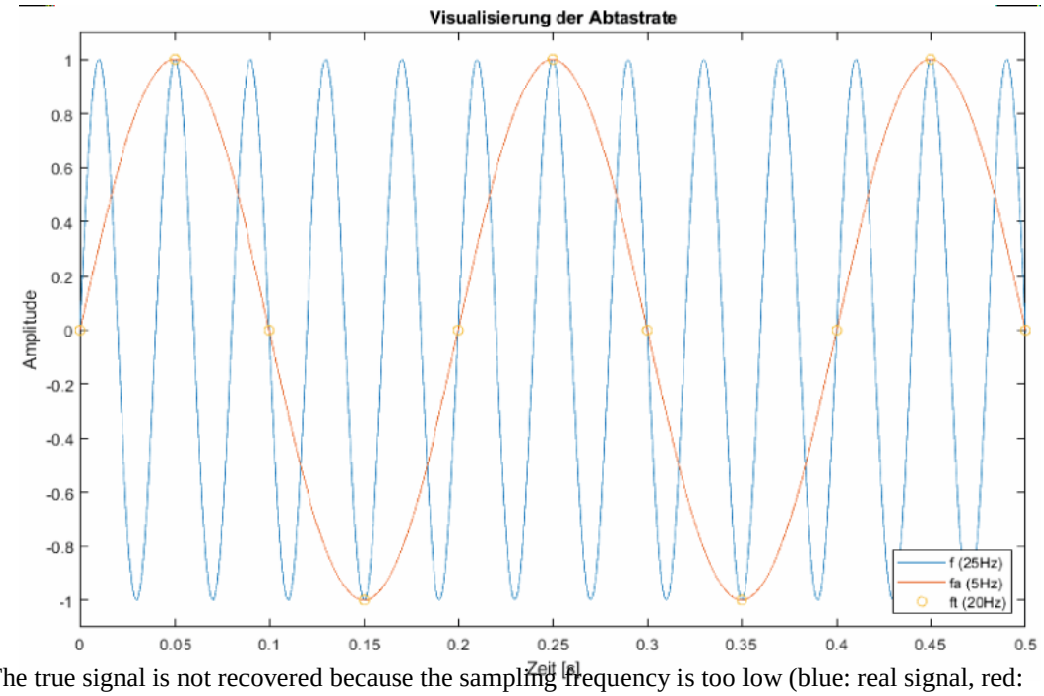

Fig. 5.2.4.2 The true signal is not recovered because the sampling frequency is too low (blue: real signal, red: data).

In contrast, when it is sampled only every 0.05 seconds (frequency of 20Hz), a second frequency of 5 Hz also meets all the data points that are created by the sampling (Figure 5.2.4.2). This frequency is called an alias frequency to the true signal of 25 Hz. It appears in the data and distorts the results of the measurements. Mathematically, we can derive a condition our sampling frequency has to fullfill to prevent the ocurrence of these alias signals:

In a marine environment, there are several sources of noise that are recorded by the hydrophones and that affect the data negatively. Most noticeable are low frequency signals created by the engine and the propeller of the ship and the waves on the ocean surface. Also, the maximum sampling frequency is subject to technical limitations, making it difficult to record very high signals without producing alias functions. Therefore, filtering is implemented to reduce the data to the midrange frequencies that are relevant for further processing and evaluation.

The most widely used filters are analogue parts consisting of simple circuits encompassing capacitators, resistors and coils. When signals of certain frequencies are fed into those filters, the impedance diverges, effectively muting the current. Generally, it would be desirable for the filters to have a box-like transfer function with very steep flanks. This would allow for ideal seperation of useable and unusable frequencies. This though is not realizable in a practical way. Also, such a transfer function would lead to problems when it is fourier-transformed from frequency space to time space, as the fourier transform of a box function is the sinc. Applying an ideal filter would thus create misleading interference when analyzing the data. Therefore, the actual filters provide transfer functions with more or less inclined edges (Figure 3.3.3).

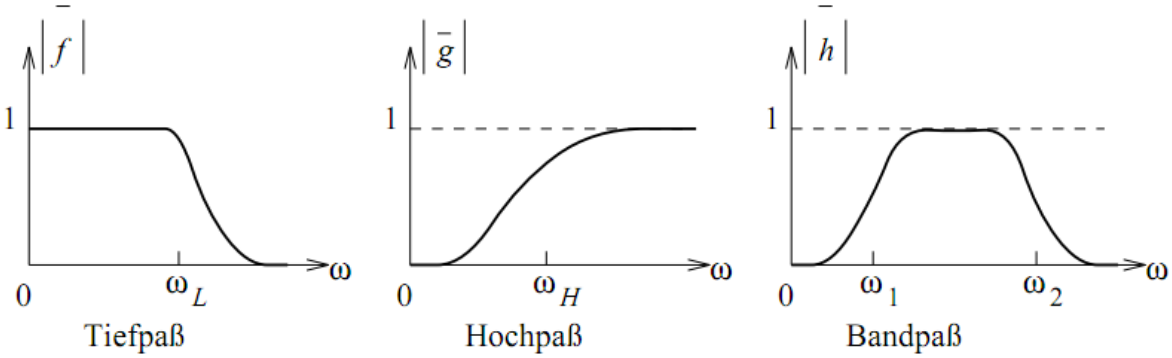

Fig.5.2.4.3 Different types of filters that can be applied to the data. Source: Dirk Gajewski: Angewandte Seismik (Script).

The streamers that are used in marine seismic exploration range from multiple hundreds of meters length up to multiple kilometers (Figure 5.2.2.1). They are equipped with hydrophones in with fixed gaps in between. When measuring, every shot of the airgun is recorded by every hydrophone in varying intensity, depending on the distance to the source and the composition of the sea floor. Now, to refine and reduce the data, it is necessary to combine the signals of different shots or of different hydrophones. There are multiple ways of going about this.

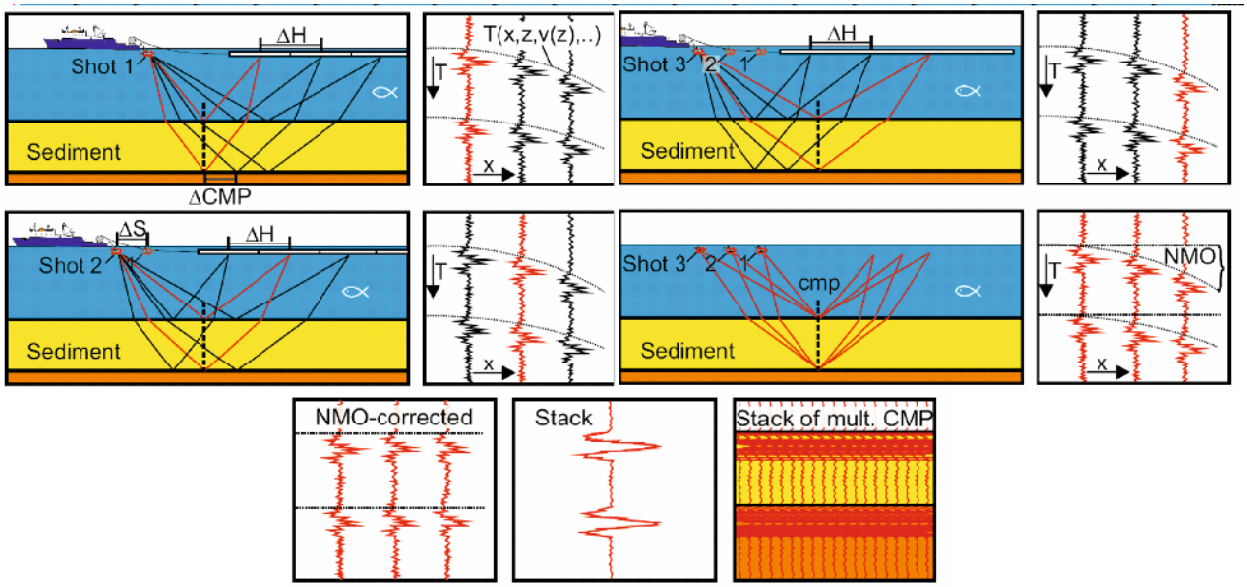

Fig. 5.2.4.4 CMP-Sorting (after Hübscher and Gohl, 2014).

Most widely used for sea floor exploration though is the common midpoint gather, or CMP gather (Fig. 5.2.4.4). Here, all pairs of shots and receivers that reached the mid-point between shot and receiver coordinates are stacked. This means that the point is sampled multiple times. When creating the stack, the usable signals interfere constructively, while noise cancels itself out. Thus, a more detailed and reliable picture of the ground is created. In theory, every point on the below the route of the research vessel is targetted multiple times by source-receiver-pairs. In a real measurement though, problems arise: Neither does the vessel move along a perfectly straight line, nor can it keep a completely constant pace. To compensate this, the sea floor is overlaid virtually with a predefined grid. All CMP's in the same grid space are now combined

into a single idealized CMP, and the data is stacked as described above. This process is called seismic binning.

Different velocities are important when analysing seismic data. The interval velocity is the average velocity in an interval between two reflectors. The RMS-velocity for a given layer refers to its root-mean-square velocity.

The analysis of seismic reflection data involves a Normal Moveout (NMO) correction. This procedure aligns the hyperbolic trajectory of reflection events. The correct determination of a specific parameter, the so-called NMO-velocity, is indispensable for this procedure.

In a horizontally stratified earth, the NMO-velocity of a specific layer equals its RMS-velocity. Velocity analysis aims at constructing a RMS velocity function to subsequently carry out the NMO correction. The analysis is carried out for a range of selected CMP gathers.

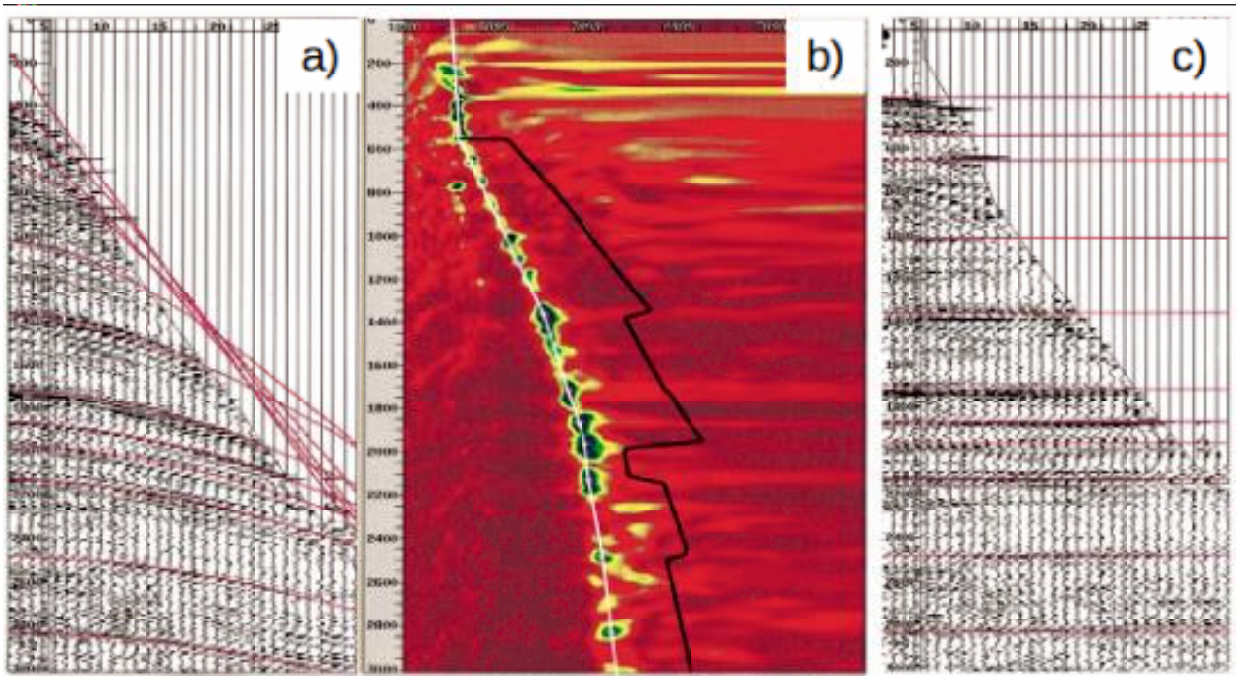

Fig. 5.2.4.5 Velocity analysis for a CMP-gather. Left: CMP-gather with modelled travel times. Midlle: Semblance with picked velocity function (Vnmo in white, Vint in black). Right: CMP-gather after nmo-correction (Yilmaz, 2001).

The RMS-velocities are determined by using of the concept of local coherence. The aim is to obtain picks that correspond to the best coherency of the hyperbolic trajectories. A quantitative measure of coherency provides the Semblance, which is a normalized cross-correlation function. Semblance values are calculated for a range of physically plausible, constant RMS-velocities. In the resulting velocity spectrum, the best-fitting RMS-velocity for a given time corresponds to the peak amplitude of the semblance value. Between the manually picked RMS velocities, a linear interpolation is carried out to obtain the required velocity function. Once the best-fitting RMS-velocities are known, the interval velocities can be calculated.

In Figure 5.2.4.5 a), a CMP-gather is shown. Its velocity spectrum is displayed by figure 3.3.5 b). The white curve shows the picked RMS velocity function. The black curve represents the interval velocities, respectively. Figure 3.3.5 c) shows the CMP-gather after the application of the NMO-correction. Apparently, the reflection events are considerably flattened. After the application of the NMO-correction, a CMP stack is obtained by summing over the offset axis.

During the stacking process, the NMO-corrected reflected energy sums up constructively over the entire spread length while unwanted energy interferes destructively.

Generally, seismic waves lose energy while traveling through the Earth. This is due to intrinsic attenuation, spherical divergence and reflection losses. To compensate for this, an exponential gain is applied to the data. As a result, weak amplitudes that originate in deeper layers are artificially enlarged.

5.2.5 Seismic Interpretation – Fundamentals

(V. Wodtke)

Seismic interpretation takes place after the seismic data processing. In seismic interpretation, you work with the processed seismic data obtained beforehand through seismic measurements/exploration. The goal of seismic interpretation is to determine the geological framework of the processed seismic section. Seismic interpretation can be split into three main subjects, structural interpretations, stratigraphic interpretations and lithologic interpretations.

In general, the seismic section can be divided into conformities and unconformities. Conformities describe the parallel undisturbed layering of rock strata, which hint towards a continuous undisturbed sedimentation. In contrast, unconformities describe the discontinued angular layering of strata resulting from tectonic or volcanic events and erosion. While conformities are easy to identify and to interpret, it is much harder to classify unconformities. There is a big range of different unconformity classifications, the most common being the angular unconformity. These develop, when tilted sediment layers reach the surface through tectonic movement. At the surface they face erosion when the sea level drops, and they get shaped into a plane. When the sea level rises again, sediment gets deposited onto the plane. The newly created sediment layers lay horizontally on the tilted old layers.

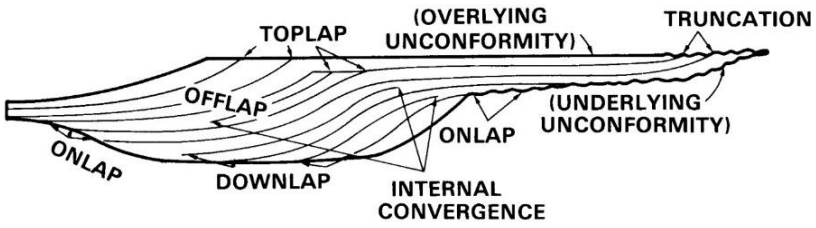

Fig. 5.2.5.1 Termination Pattern.

In the seismic section, an angular unconformity can be identified through the termination of an inclined reflection through an overlaying lesser inclined layer. This termination pattern is called “Toplap”. When the reflection terminates instead at the bottom layer, we call it “Downlap”. This can occur when inclined sediment-deposits develop at the basin margin. Another form of termination pattern appears, when reflections terminate on more steeply dipping strata or when a low-angle reflection terminates against steeper reflections. These so called “Onlaps” can develop while transgression. Due to the rise of sea level, at basin margin new sediments wash over older sediments and get deposited on top of them towards the shore. Contrary to “Onlaps” there are also offlaps, which develop while regression. Strata prograde into deeper water and terminate at the deeper basin, no longer covering the underlaying sediments.

This also results in a regressing coastline. When reflections end because of erosion or structural events, we call the termination pattern “truncation”, often easily distinguishable because of their jagged shape.

If you look at more than one single reflection termination, we can see whole reflection patterns. These can be divided into layered and unlayered reflections. Unlayered reflections include chaotic and reflection-free stratification. A chaotic stratification occurs when there are a lot of active events with much movement, reflection-free sections can occur when there are fluids.

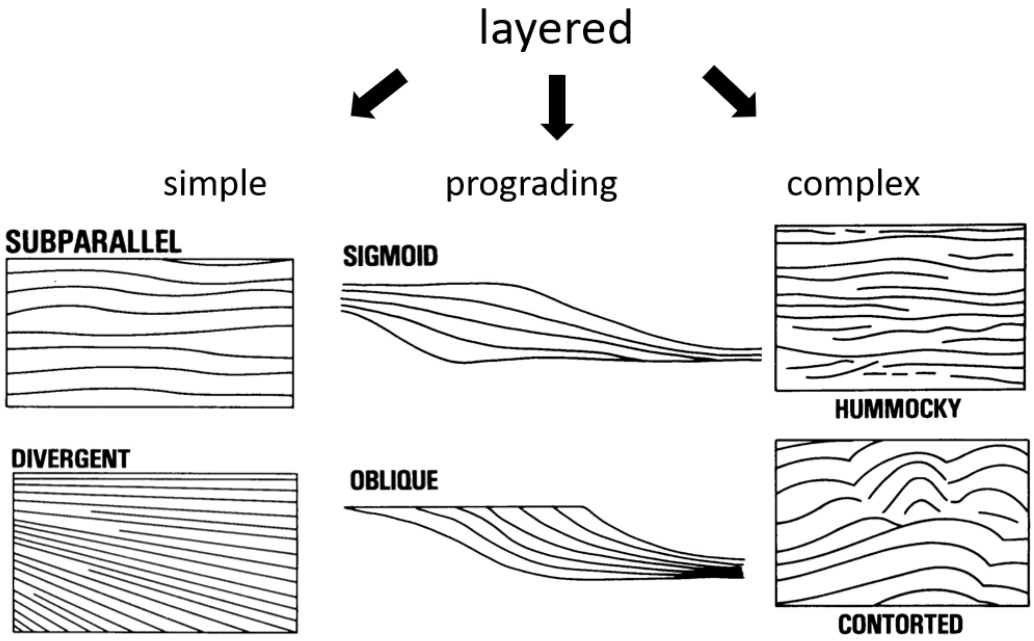

Fig. 5.2.5.2 Reflection Pattern of a layered underground.

Layered reflections can be divided into three classifications, simple, complex and progradational. Simple patterns are easy to identify and the most common. The stratification is continuously parallel or subparallel. It can also be divergent, meaning there are more parallel or subparallel reflections on one side then on the other side. There are many different complex patterns, with each referring to a special event leading up to the creation. For example, hummocky reflection patterns, random thickening and thinning of strata, are the result of crevasses, contorted patterns the result of hillside slides. The last classification, progradational patterns, are based on Clinoforms. A Clinoform is a two-dimensional surface with a sloped geometry that is characteristic of base margin strata. What is special about them is, that they have deposited at an angle and did not get tilted post-depositionary. Because of their correlation to basins, the knowledge of them is very valuable for exploration. The three most common progradational reflection patterns are sigmoidal, oblique and shingled. Typical for sigmoidal patterns is an s-shape with a downlapping character aggrading into a basin. They can be traced back to a low sediment supply and a quick basin subsidence. Oblique patterns are toplapping and are prograding into a basin, creating a plane. They only appear at water depths of 500m due to high sediment supply and low basin subsidence.

Another very important structure, especially in exploration, are anticlines. These usually occur together with synclines and they get caused by compressional stress during tectonic

processes. The difference between anticlines and synclines lies in the shape and the order of the sediment layers. Anticlines are folds with an arch-like shape and with their oldest rock-layers at its core. A syncline is the inverse of an anticline. Often anticlines are reservoirs for hydrocarbons like petroleum.

5.2.6 Seismic Interpretation – Tectonics

(Carina Dittmers)

Tectonics is a field of geodynamics describing the structure and movements of the earth's crust. That includes the movement of large-scale tectonic plates as well as local, regional and microscopic plates. Both within and between those plates tectonic faults occur. Those are distinguished in normal, reverse and strike-slip faults. Normal faults occur when the earth's crust is expanding, and the two walls have increased room to spread out in. The footwall slips downwards relative to the hanging wall at an angle. This can be detected in seismic sections as seen in this CMP depiction.

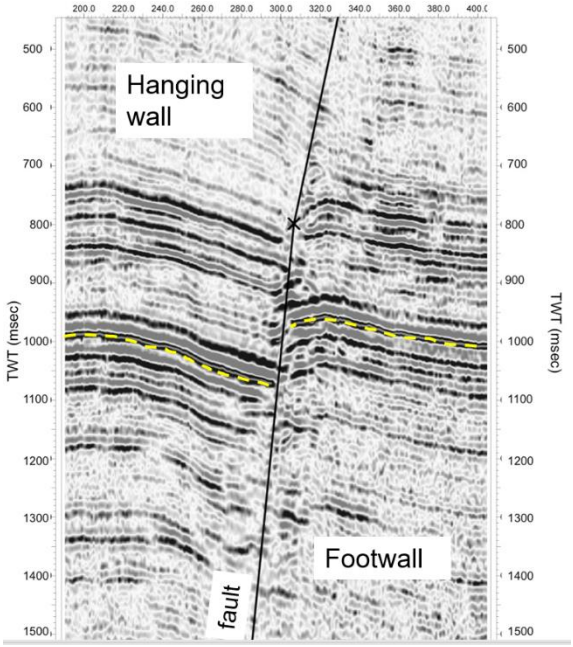

Fig. 5.2.6.1 Seismic section of a normal fault http://www.sub-surfrocks.co.uk/?page_id=387 accessed 22.06.2020.

To describe combinations of normal faults, additional terms need to be introduced. Graben and Horst are terms used to describe wall blocks that are elevated (Horst) or down-dropped (Graben) relative to each other. Listric normal faults are upward-dipping concave normal faults, synthetic normal faults dip into the same direction as the major normal fault, whereas antithetic normal faults dip into the opposite direction (see Fig. 5.2.6.2).

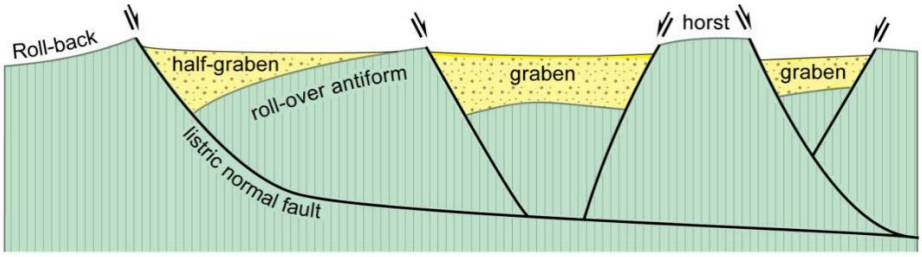

Fig. 5.2.6.2 Main components of a normal fault system (Dwonloaded from https://www.files.ethz.ch/structuralgeology/JPB/files/English/3extsyst.pdf accessed 22.06.2020.

When the crust constricts, reverse faults occur, which leads to the hanging wall being pushed upwards relative to the footwall. If the angle between them is greater than 45° it is called a thrust fault. Large-scale examples for this are the subduction zones like the Mariana trench (Ocean-Ocean-Subduction) or the Andes (Ocean-Continent-Subduction). A small-scale example is the CMP depiction below.

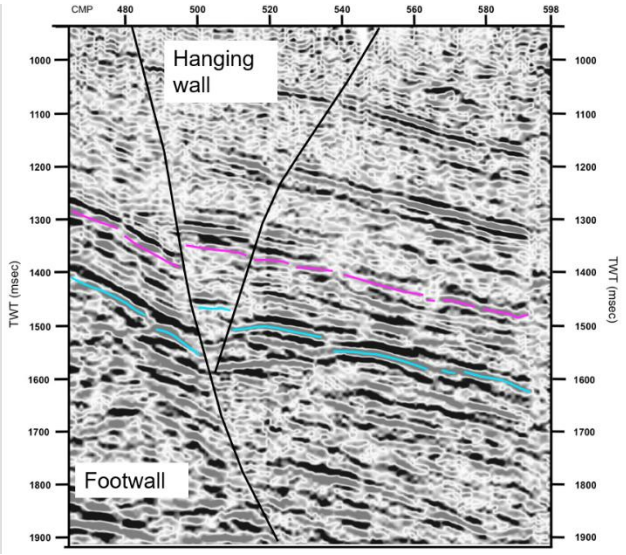

Fig. 5.2.6.3 Seismic section of a reverse fault http://www.sub-surfrocks.co.uk/?page_id=387 accessed 22.06.2020.

Strike-slip faults are horizontal faults where two walls slip relative to each other either dextral or sinistral, meaning to the left or to the right. Occurrences of this between tectonic plates are called transform-faults whereas strike-slip faults within plates are called transcurrent-faults. A commonly known example for a transform fault is the San Andreas fault in California. Strike slip faults often occur in combination with reverse or normal faults as so-called flower structures. A negative flower structure is a combination of strike-slip faults and normal faults, whereas a positive flower structure is a combination with a reverse fault as seen below.

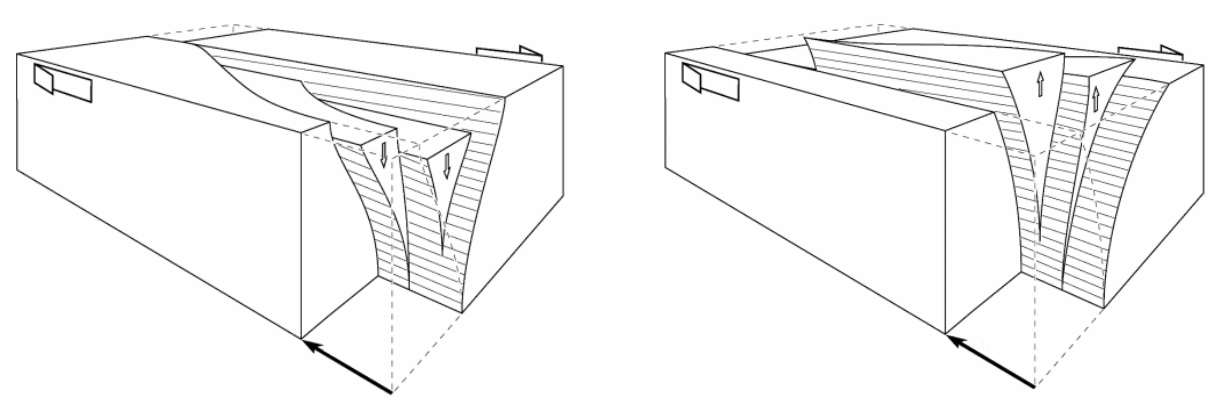

Fig. 5.2.6.4 Depiction of negative (left) and positive (right) flower structures https://www.files.ethz.ch/structuralgeology/JPB/files/struk/3Verwerf.pdf accessed 22.06.2020 .

Flower structures can also be detected using seismic methods as seen in Fig. 5.2.6.5, which shows an example of negative flower structures.

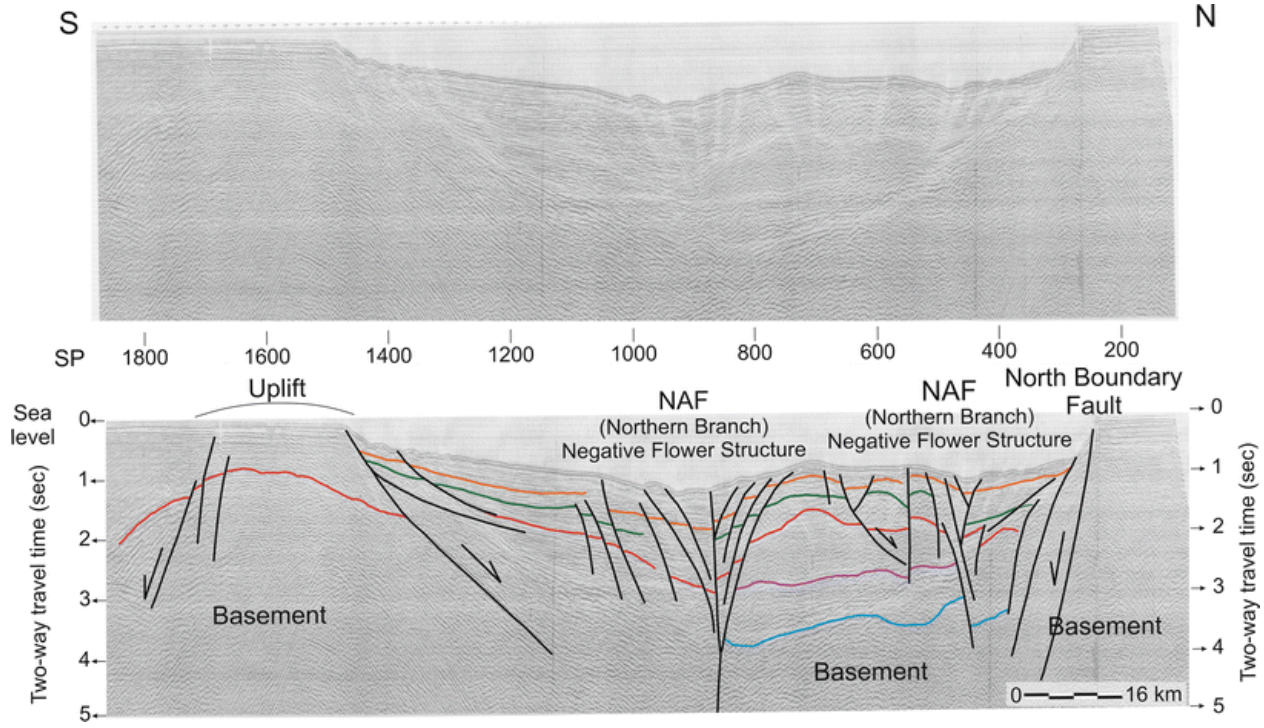

Fig. 5.2.6.5 Seismic section showing negative flower structures, raw and interpreted https://media.springernature.com/original/springer-static/image/art%3A10.1007%2Fs11001-010-9083-z/MediaObjects/11001_2010_9083_Fig3_HTML.gif accessed 24.06.2020.

Tectonics are responsible for creating many different topographical structures including mountains. There are two types of mountains, the fold mountains and fault-block mountains. The former is formed when the earth's crust is constricted and as a result the edges of two plates move upwards. Examples for this are the Alps and the Himalayans. The latter forms when a solid piece of crust breaks and the resulting blocks settle on different heights relative to each other. An example for this is the Harz mountain range.

5.2.7 Magnetic

(K.J. Uhl)

The most common used magnetometers are the Fluxgate magnetometer and the Proton precession magnetometer. The Fluxgate magnetometer which measures a vector, works with an AC current which is applied on two ferromagnetic cores with a primary and secondary coil wrapped around it. In a field-free space the voltage of the two cores cancel each other out. In a non-field-free space the cores are not saturated at the same time. This has an impact on the voltage and therefore it does not immediately equal zero. To measure a vector field with three axes it is necessary to use three Fluxgate-Magnetometers. [1]
The Proton precession magnetometer, also called Overhauser magnetometer measures a scalar. It is based on a liquid (high in protons i.e. water or paraffin) in a non-magnetic bowl which is wrapped by a coil and applies a strong magnetic field to the liquid. The nuclear spin of the protons is now redirected by the applied magnetic field. By turning the magnetic field off the nuclear spin is getting redirected by the present magnetic field (as it can not be the same direction as the applied magnetic field). This process is called the Larmor-Precision. Through the precision Electro-magnetic radiation is released. This radiation creates a voltage in the coil, which can then be measured.[1]

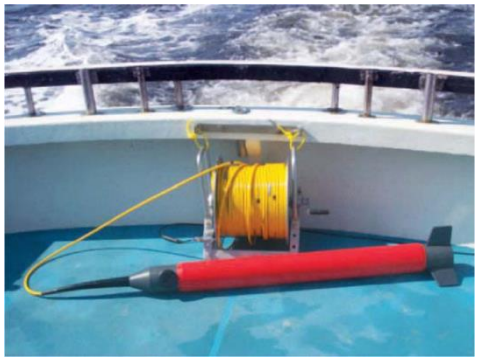

Figure 5.2.7.1 SeaSPY at the stern of the ship.

The SeaSPY, which was being used on the Alkor 545, is a marine magnetometer and works with three Proton precession magnetometer. It is either used as a magnetometer or gradiometer depending on its setup. A gradiometer measures the difference between two magnetic fluxes. Important is to ensure that the influence by the ship on the measurements is minimized. Normally this is guaranteed by creating a distance about three times the ships length between the SeaSPY and the ship. [2]

The Earth's magnetic field is divided into three different fields: the Anomaly field, the Variation field and the Total field. The goal of most expeditions is to detect differences in the Anomaly field which is affected by local geological structures such as basalt, mineral deposits and metamorphic rock. Additionally, breakouts in the magnetic field are caused by ship wrecks or pipelines.To suppress the Total field and Variation field it is necessary to apply corrections. As the Earth's magnetic field varies over time (long periods: years and decades), and with location, it is necessary to subtract the International Geomagnetic Reference Field (IGRF) from the data for correct results. The IGRF is a model of the Earth's magnetic field and is updated every five years. The Variation field which changes within seconds due to solar storms and their impact on the ionosphere. To filter the impact of the Variation field from the data it is either necessary to have a base station in the area where the measurements are conducted [3] or to measure with a Gradiometer. As the Gradiometer just measures the difference between the two Magnetometer there is no need to apply any corrections. A magnetic survey at sea can be used to

determine the age of the sea floor and can at the same time prove sea floor spreading. Furthermore, it can be used to detect pipelines and ship wrecks.

5.2.8 Gravity

(Ji In Chung)

Gravity is usually measured in units of acceleration. In the SI system of units, the standard unit of acceleration is 1 m/s^2 but in gravimetry, the unit Galileo (Gal) is more frequently used, which equals 1 cm/s^2. The average of Earth's gravitational acceleration equals 978 Gal. 99.4 percent of Earth's gravitational field is made by Earth's gravitational pull, and the other 0.6 percent by the rotation of Earth.

Earth is often represented as a sphere with a smooth surface, but in reality, it is an ellipsoid with an irregular surface. Influences such as winds, rain, and tides resulted in topological differences, which affect the gravitational acceleration of the planet. If one were to only consider the influence of the Earth's gravity and rotation alone it would take the shape of an ellipsoid with a relatively smoother surface. This is called the geoid. Gravitational force acts perpendicular to every point on the geoid. The height of the surface of the geoid is defined by gravity: the surface is higher than the reference ellipsoid when a positive gravity anomaly exists and lower wherever there is a negative gravity anomaly.

Gravity is measured by a gravimeter. There are two types of gravimeters: an absolute gravimeter and a relative gravimeter. Absolute gravimeters calculate the acceleration of a freefalling mass in vacuum and give the measurement of absolute gravity in the unit Gal. Absolute gravity is used for calibrating relative gravimeters.

The basic structure of a relative gravimeter is a spring with a fixed mass. It measures local gravity by measuring the stretch of the spring as the weight of the mass changes with the change in gravity. Relative gravimeters need to be regularly calibrated at a base station where the absolute gravity is known.

The first step of a gravimetric survey is route planning. The order in which the stations are measured might have a significant impact on the budget and efficiency of the survey, so it is important to plot the proposed observation stations and route before the survey. Surveys may be influenced by geology so when planning station spacing one should consider the existing gravity anomaly patterns. However in marine surveys due to influences such as tide and currents, the exact positioning of stations might experience some difficulties. By keeping the time and distance between each station to a minimum the risk of severe weather changes and the effect of drift can be reduced.

Gravity is affected by the shape and rotation of the Earth. To reduce the effects of these influences gravity corrections are conducted on observed gravity, abbreviated as g_{obs}. The usual corrections are tidal correction, drift correction, free-air correction, Bourger correction, and Eötvös correction.

Tidal corrections account for the time-varying gravitational force due to the change in the distance from Earth to the Sun and the Moon. Most of the modern gravimeters are equipped to routinely make tidal corrections. The drift correction is usually made after the tidal correction. The instrument drift is the residual time varying gravity after the tidal variation is removed.

Instrument drift is variations caused by the mechanical, thermal, and electrical changes in the gravimeter with time.

The free-air correction accounts for gravity variations caused by elevation differences between the base station and measurement points. The equation for free-air correction is

$$\Delta g_{FA} = g_{obs} - g_N + z\ (0.3086\ \text{mGal}) \quad (1)$$

where Δg_{FA} is the free-air gravity anomaly, g_N the theoretical gravity, and h the elevation of the station from the geoid.

The Bouger correction accounts for the elevation and density of rock between the measurement point and the reference ellipsoid. If the measurement point is located above the reference ellipsoid, the excess mass of rock between them increases the gravity.

$$\Delta g_B = \Delta g_{FA} - \rho\ h\ (0.0419\ \text{mGal}) \quad (2)$$

Here Δg_B represents the Bouguer anomaly, and ρ the density of slab in between.

The Bouguer correction ($0.0419\rho h$) at sea can be written as

$$BC_s = 0.0419(\rho_w - \rho_c)h_w \quad (3)$$

where ρ_w is the density of seawater, ρ_c the density of Earth's crust, and h_w the water depth below the measurement point.

Lastly, the Eötvös correction is considered when using a moving meter. Due to the Eötvös effect, gravitational force varies depending on the direction of the movement: When traveling east due to Earth's rotation and centrifugal force the gravity increases, whereas when traveling west the gravity decreases. The formula for Eötvös correction is

$$E = 7.507 * v_S * \cos(\alpha) * \sin(\beta) + 0.004\ v_S^2 \quad (4)$$

where v_S is the velocity of the ship in knots, α is the latitude, and β is the track of the ship.

5.5 Expected Results

(C. Hübscher and AL545 Shipboard Scientific Party)

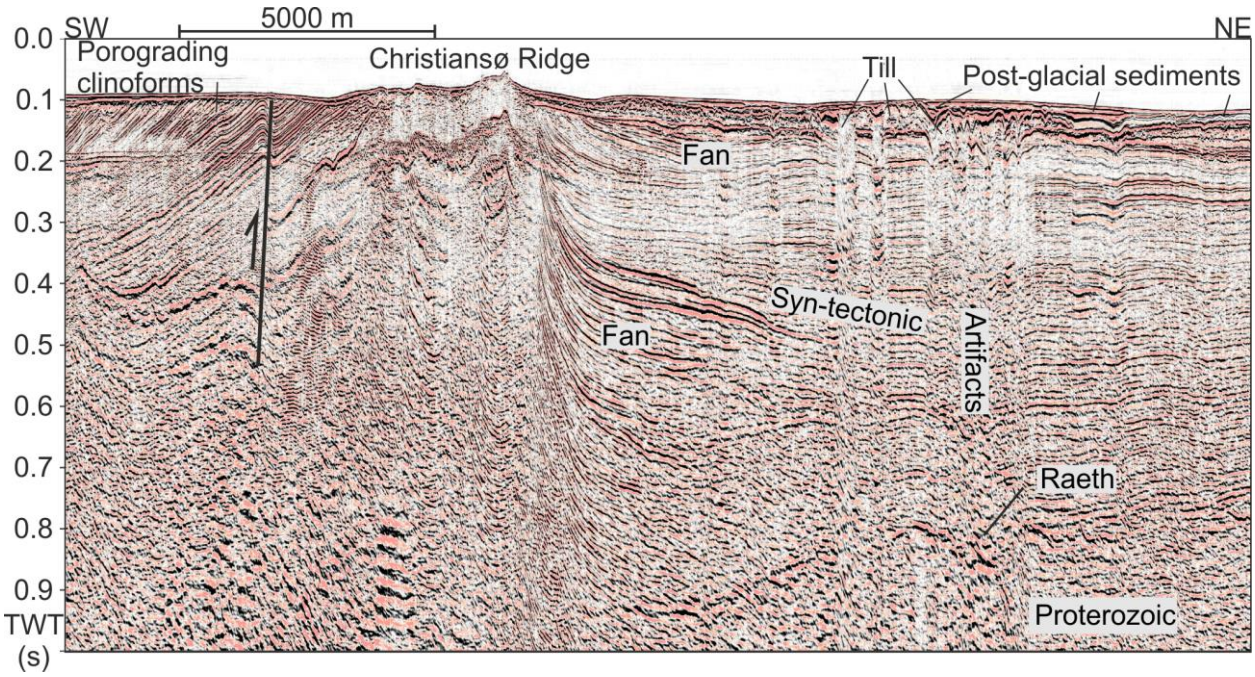

Fig. 5.5.1 Seismic data instance from Bornholm area, showing inversion tectonics and related fan deposition.

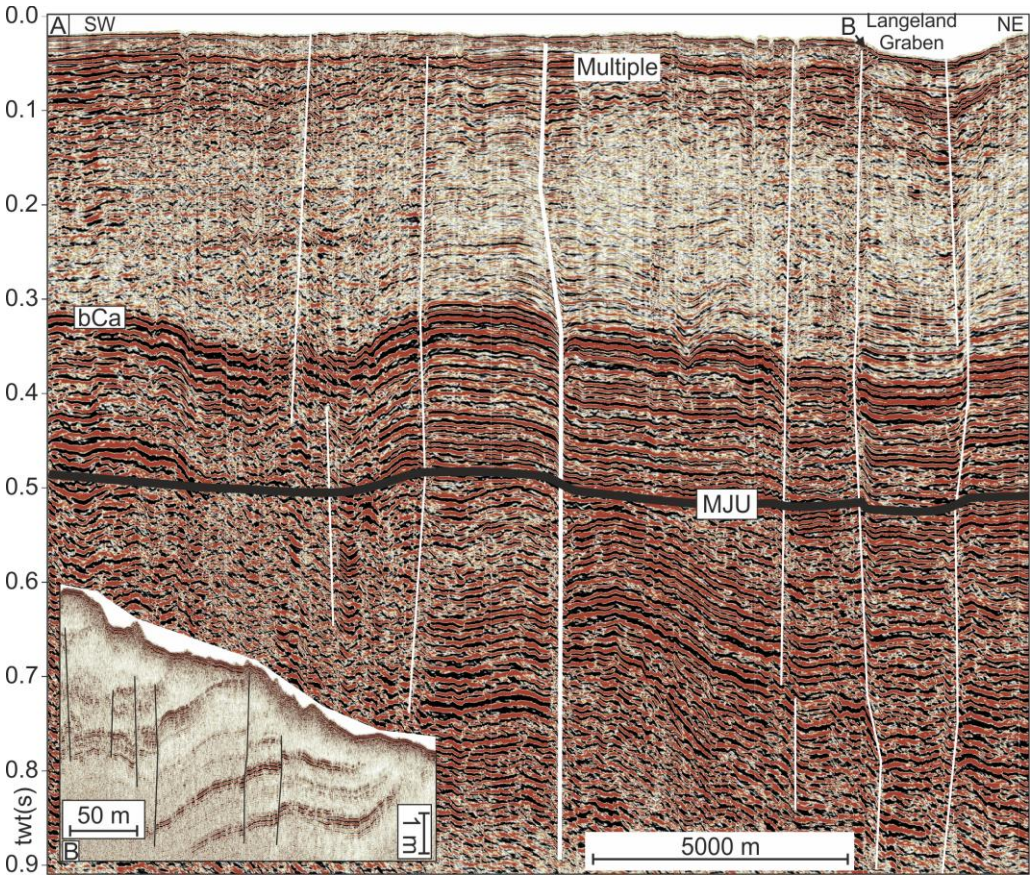

Fig. 5.5.2 A) Seismic profile across Langeland Graben. White lines indicate faults. bCa: Base Campanian; MJU: Mid-Jurassic unconformity. B) Parametric echosounder instance from Langeland Graben margin. Location indicated in a).

6 Station List AL526

6.1 Profile Station List

Station Number	MCS Profile	Start Date	Start Time (UTC)	Start Latitude (°N)	Start Longitude (°E)	End Date	End Time (UTC)	End Latitude (°N)	End Longitude (°E)	Length (km)
AL545_1-2	TP(1)	19.09.20	6:52	55°04.1‘	14°19.1‘	19.09.20	07:34	55°06.3‘	14°22.2‘	5,5
AL545_2-2	02	19.09.20	07:34	55°06.3‘	14°22.2‘	19.09.20	14:48	55°28.8‘	14°53.8‘	56,9
AL545_2-2	03	19.09.20	15:14	55°27.9‘	14°55.6‘	19.09.20	16:41	55°22.8‘	14°50.8‘	21,2
AL545_2-2	04	19.09.20	17:57	55°26.9‘	14°50.1‘	19.09.20	01:25	55°05.4‘	15°25.9‘	61,5
AL545_2-2	05	20.09.20	02:16	55°07.4‘	15°26.2‘	20.09.20	04:40	55°14.5‘	15°14.5‘	24,9
AL545_2-2	06	20.09.20	05:35	55°17.7‘	15°16.8‘	20.09.20	08:00	55°10.4‘	15°28.6‘	23,8
AL545_2-2	07	20.09.20	08:44	55°12.1‘	15°29.7‘	20.09.20	10:13	55°16.2‘	15°21.9‘	16,9
AL545_2-2	08	20.09.20	10:53	55°17.9‘	15°23.2‘	20.09.20	11:57	55°14.5‘	15°29.2‘	18,8
AL545_2-2	09	20.09.20	13:08	55°18.6‘	15°31.3‘	20.09.20	17.15	55°30.4‘	15°06.7‘	33,9
AL545_2-2	10	20.09.20	17:39	55°31.3‘	15°08.7‘	20.09.20	21:26	55°20.6‘	15°32.2‘	37,6
AL545_2-2	11	20.09.20	22:09	55°21.1‘	15°32.0‘	21.09.20	08:33	55°49.6‘	15°10.7‘	62,7
AL545_4-2	12	22.09.20	13:45	54°49,9‘	15°06,0‘	22.09.20	22:02	55°24,7‘	15°30,5‘	69,8
AL545_4-2	13	22.09.20	22:36	55°25,1‘	15°27,2‘	23.09.20	02.15	55°09,8‘	15°16,8‘	30,6
AL545_4-2	14	23.09.20	03:00	55°11,2‘	15°13,1‘	23.09.20	06:25	55°15,6‘	15°24,0‘	32,5
AL545_4-2	15	23.09.20	09:28	55°30,3‘	15°13,8‘	23.09.20	13:00	55°16,2‘	15°59,8‘	30,0
AL545_4-2	16	23.09.20	13:51	55°18,1‘	14°56,2‘	23.09.20	17:14	55°31,2‘	15°09,7‘	28,1
AL545_4-2	17	23.09.20	18:01	55°31,4‘	15°04,7‘	23.09.20	20:48	55°20,3‘	14°53,8‘	23,6
AL545_4-2	18	23.09.20	22:30	55°19,6‘	15°04,1‘	24.09.20	01:00	55°27,5‘	14°50,3‘	20,6
AL545_4-2	19	24.09.20	02:18	55°28,4‘	14°58,2‘	24.09.20	03:59	55°23,0‘	15°07,7‘	14,1
AL545_4-2	20	24.09.20	04:22	55°24,0‘	15°07,9‘	24.09.20	05:48	55°28,5‘	15°00,0‘	11,9
AL545_4-2	21	24.09.20	06:35	55°30,8‘	15°04,0‘	24.09.20	08:19	55°25,4‘	15°12,6‘	14,2
AL545_5-2	22	25.09.20	12:48	54°57,9‘	11°02,0‘	25.09.20	15:05	55°07,8‘	11°02,1‘	19,0
AL545_5-2	23	25.09.20	15:24	55°07,7‘	11°04,3‘	25.09.20	17:48	54°57,7‘	10°59,6‘	19,3
AL545_5-2	24	25.09.20	18:13	54°57,9‘	11°01,6‘	25.09.20	20:29	55°07,7‘	11°05,8‘	18,8
AL545_5-2	25	25.09.20	20:52	55°7,6‘	11°03,7‘	25.09.20	23:07	54°57,9‘	10°59,3‘	18,8
AL545_5-2	26	25.09.20	23:33	54°57,8‘	11°01,1‘	25.09.20	01:49	55°07,7‘	11°05,5‘	19,1
AL545_5-2	27	26.09.20	02:15	55°07,6‘	11°03,4‘	25.09.20	04:38	54°57,7‘	10°58,9‘	19,1
AL545_5-2	28	26.09.20	06:01	54°57,5‘	11°00,8‘	26.09.20	07:16	55°07,2‘	11°5,09‘	18,8
AL545_5-2	29	26.09.20	07:42	55°7,6‘	11°03,1‘	26.09.20	09:55	54°57,8‘	10°58,5‘	18,9
AL545_5-2	30	26.09.20	10:21	54°57,87‘	11°00,4‘	26.09.20	12:36	55°07,7‘	11°04,7‘	19,0
AL545_5-2	31	26.09.20	12:59	55°07,8‘	11°02,8‘	26.09.20	15:20	54°57,8‘	10°58,2‘	19,2
AL545_5-2	32	26.09.20	15:42	54°57,9‘	11°00,1‘	26.09.20	17:59	55°07,7‘	11°04,4‘	18,7
AL545_5-2	33	26.09.20	18:24	55°07,6‘	11°02,4‘	26.09.20	20:38	54°57,8‘	10°57,6‘	19,2
AL545_5-2	34	26.09.20	21:23	54°58,6‘	10°53,5‘	26.09.20	22:39	54°59,6‘	11°03,3‘	10,7
AL545_5-2	35	26.09.20	22:58	55°00,8‘	11°03,7‘	27.09.20	00:27	54273	10°53,3‘	12,7
AL545_5-2	36	27.09.20	00:59	55°07,7‘	10°58,5‘	27.09.20	03:05	54°57,9‘	10°53,3‘	19,3
AL545_5-2	37	27.09.20	03:53	54°58,0‘	10°55,6‘	27.09.20	06:02	55°07,7‘	11°00,5‘	18,9
AL545_5-2	38	27.09.20	06:27	55°7,6‘	10°58,8‘	27.09.20	08:40	54°57,9‘	10°53,7‘	18,8
AL545_5-2	39	27.09.20	09:03	54°57,9‘	10°56,0‘	27.09.20	11:15	55°07,7	11°00,8‘	19,0
AL545_5-2	40	27.09.20	11:34	55°07,8‘	10°59,2‘	27.09.20	14:00	54°57,7‘	10°54,0‘	19;4
AL545_5-2	41	27.09.20	14:24	54°58,0‘	10°56,3‘	27.09.20	16:22	55°07,8‘	11°01,2‘	19,0
AL545_5-2	42	27.09.20	16:44	55°07,7‘	10°59,5‘	27.09.20	19:21	54°57,9‘	10°54,5‘	19,0
AL545_5-2	43	27.09.20	19:42	54°58,0‘	10°56,8‘	27.09.20	21:48	55°7,7‘	11°1,5‘	18,8
AL545_5-2	44	27.09.20	22:06	55°07,8‘	11°0,1‘	28.09.20	0:36	54°57,9‘	10°54,9‘	19,2
AL545_5-2	45	28.09.20	0:56	54°57,9	10°57,9‘	28.09.20	3:07	55°7,9‘	11°1,9‘	19,2
AL545_5-2	46	28.09.20	3:40	55°7,7‘	11°0,2‘	28.09.20	6:16	54°57,9‘	10°55,2‘	18,9
AL545_5-2	47	28.09.20	6:54	54°58,0‘	10°57,6‘	28.09.20	8:52	55°7,8‘	11°2,2‘	18,7

7 Data and Sample Storage and Availability

All data will be provided upon request after 1. September 2023. As soon as there is a national data base for marine seismic data, data will be uploaded. For the time being, data are stored in facilities of Institute for Geopyhsics, University of Hamburg. Contact: Christian.huebscher@uni-hamburg.de

8 Acknowledgements

We thank master Marc Petrokowski and his crew for their great support during the cruise. Sven Winter is thanked for the excellent technical preparation of the equipment. We further thank all German and Danish authorities which supported the diplomatic clearance.

9 References

Al Hseinat, M., & Hübscher, C. (2017). Late Cretaceous to recent tectonic evolution of the North German Basin and the transition zone to the Baltic Shield/southwest Baltic Sea. Tectonophysics, 708, 28–55.

Andersen,T.R., Westergaard, J.H., & Pytlich, A. (2016). Delineation of fault systems on langeland, Denmark based on AEM data and boreholes. ASEG-PESA-AIG 25th Geophysical Conference Extended Abstracts, 1-6, Adelaide, Australia.

Dragoset, W.H. (1990). Air-gun array specs: A tutorial, 9 p.

Hübscher, C., Gohl, K. (2014). Reflection / Refraction Seismology. Encyclopedia of Marine Geosciences. DOI 10.1007/987-94-007-6644-0_128-1

Huster, H., Hübscher, C., Seidel, E. (2020). Impact of Late Cretaceous to Neogene plate tectonics and Quaternary ice loads on supra salt deposits at Eastern Glückstadt Graben, North German Basin.

Sanborns' Baltic Sea Map Page, 08.10.2020. http://www.thesanborns.com/Balticsea/map-da.jpg.

Yilmaz, O. (2001). Seismic Data Analysis: Processing, Inversion, and Interpretation of Seismic Data: Processing, Inversion, and Interpretation of Seismic Data, 2027 p.